



RESEARCH ARTICLE

10.1029/2022JA030548

Occurrence Rates of Electromagnetic Ion Cyclotron (EMIC) Waves With Rising Tones in the Van Allen Probes Data Set

K. Sigsbee¹ , C. A. Kletzing¹ , J. Faden¹, and C. W. Smith²

¹Department of Physics and Astronomy, University of Iowa, Iowa City, IA, USA, ²Institute for Earth, Oceans and Space, University of New Hampshire, Durham, NH, USA

Key Points:

- Electromagnetic ion cyclotron (EMIC) waves were observed about 2.4% of the time but EMIC waves with rising tones were only observed 0.2% of the time
- Occurrence rates for H+, He+, and O+ EMIC waves and waves with rising tones were determined as functions of L and magnetic local time and R_{XY} and Z SM
- EMIC waves with rising tones were most likely to be observed in the noon and dusk sectors from $4 < L < 6$

Correspondence to:

K. Sigsbee,
kristine-sigsbee@uiowa.edu

Citation:

Sigsbee, K., Kletzing, C. A., Faden, J., & Smith, C. W. (2023). Occurrence rates of electromagnetic ion cyclotron (EMIC) waves with rising tones in the Van Allen Probes data set. *Journal of Geophysical Research: Space Physics*, 128, e2022JA030548. <https://doi.org/10.1029/2022JA030548>

Received 13 APR 2022
Accepted 11 JAN 2023
Corrected 20 FEB 2023

This article was corrected on 20 FEB 2023. See the end of the full text for details.

Abstract In Fourier time-frequency power spectrograms of satellite magnetic field data, electromagnetic ion cyclotron (EMIC) waves may feature discrete, rising tone structures that rapidly increase in frequency. Using data from the Van Allen Probes Electric and Magnetic Field Instrument Suite and Integrated Science (EMFISIS) fluxgate magnetometer, we conducted a statistical study of EMIC waves from September 2012 through June 2016. We compared the occurrence rates and spatial distributions for all EMIC waves with those for rising tone EMIC waves as a function of magnetic local time (MLT) and L shell, as well as a function of R_{XY} and Z in solar-magnetic (SM) coordinates. Overall, EMIC waves occurred during 2.4% of the time period considered, but rising tone EMIC waves were only found during 0.2% of the time period considered. About 7%–8% of the minutes of orbital coverage with H+ or He+ band EMIC waves had rising tones. The regions of peak occurrence rates for H+ and He+ band waves, as well as waves with rising tones, were found in the noon and dusk sectors for $4 < L < 6$. The preferred regions for H+ waves as a function of R_{XY} and Z SM suggest an association with magnetospheric compressions near noon and interactions between plumes and the ring current near dusk. Peak occurrence rates for O+ band waves were found between $2 < L < 4$ at all MLT, and over a wide range of L shells near dusk. No rising tones were found in the O+ band.

Plain Language Summary Using Explorer 1 data in 1958, James Van Allen discovered Earth is surrounded by donut-shaped rings of high-energy electrons and ions, now called the radiation belts. NASA launched the twin Van Allen Probes in 2012 to study how electromagnetic waves regulate the strength of the radiation belts. Radio frequency chorus waves are generated by lower-energy radiation belt electrons and accelerate them to velocities near light speed. These “killer electrons” damage satellite electronics and pose a health risk to astronauts. Chorus waves feature chirp-like rising and falling tones that sound like bird songs when played as audio. Electromagnetic ion cyclotron (EMIC) waves with frequencies of 1–4 cycles per second can remove high-energy electrons from the radiation belts. EMIC waves are generated by hydrogen, helium, and oxygen ions trapped in Earth's magnetic field and can have chirp-like rising tones similar to chorus, but they are far below the frequency range of human hearing. Using Van Allen Probes data, we compared the occurrence rates and spatial distributions of EMIC waves with rising tones and EMIC waves without rising tones. This will advance our understanding of processes that remove “killer electrons” and cause Earth's radiation belts to vary in strength during geomagnetic storms.

1. Introduction

Electromagnetic ion cyclotron (EMIC) waves observed by satellites in Earth's magnetosphere are electromagnetic emissions that occur in frequency bands defined by the gyrofrequencies of the magnetospheric ion species. The occurrence rates and properties of these waves are strongly affected by plasma composition (e.g., Cornwall & Schulz, 1971; Gomberoff & Neira, 1983; Kozyra et al., 1984; Denton et al., 2014; Lee et al., 2017). Most studies have focused on O+, He+, and H+ band waves, but it is also theoretically possible for EMIC waves to occur in a frequency band defined by the N+ gyrofrequency (Bashir & Ilie, 2018). An example of EMIC waves in the N+ band was recently reported on the Van Allen Probes (Bashir & Ilie, 2021). In linear theory, EMIC waves are generated by the temperature anisotropy of magnetospheric ions (Cornwall, 1965). Magnetospheric compressions are potential sources of ion temperature anisotropy for driving EMIC waves (McCollough et al., 2010, 2012; Usanova et al., 2008, 2010). Increases in the density of hot anisotropic ions associated with injections can also drive EMIC waves (Remya et al., 2018). Studies of cyclotron instabilities have shown that EMIC waves can be produced by various types of anisotropic particle distributions, such as ring-like proton distributions near the Alfvén speed (Fok et al., 2016; Mithaiwala et al., 2013) or by Kappa-type distributions (Mace et al., 2011). The

© 2023. The Authors.

This is an open access article under the terms of the [Creative Commons Attribution-NonCommercial-NoDerivs License](https://creativecommons.org/licenses/by/4.0/), which permits use and distribution in any medium, provided the original work is properly cited, the use is non-commercial and no modifications or adaptations are made.

basic linear theory says that when EMIC waves are observed in space, they should be left-hand polarized, transverse magnetic field fluctuations. While this is sometimes true, observations have been made of linear and even right-handed waves in the EMIC wave frequency bands (e.g., Anderson et al., 1992b; Min et al., 2012; Sakaguchi et al., 2013). Linearly and right-hand polarized EMIC waves may be generated by mode conversion processes (Kim et al., 2015; Sakaguchi et al., 2013), but another possibility is that different wave polarizations are caused by variations in plasma composition (Min et al., 2012).

EMIC waves have been established as one of several types of radio and plasma waves that play critical roles in the energization and depletion of the radiation belts and ring current (e.g. Horne & Thorne, 1994; Jordanova et al., 2001; Thorne, 2010; Thorne & Horne, 1994; Thorne & Kennel, 1971). EMIC waves were mainly thought to scatter only the highest energy electrons as the minimum resonant energies for wave-particle interactions with EMIC waves are usually well above 2 MeV (Meredith et al., 2003). However, Meredith et al. (2003) also showed that localized regions of high plasma density and/or low magnetic field could reduce the minimum resonant energy for waves just below the H⁺ or He⁺ gyrofrequencies. More recent work has confirmed that EMIC waves can result in precipitation of sub-MeV electrons with energies around 300–400 keV (Hendry et al., 2017; Ukhorskiy et al., 2010). Satellite observations show EMIC waves are effective at producing localized pitch angle scattering of electrons and protons (Bingley et al., 2019; Sigsbee et al., 2020; Usanova et al., 2014). However, the extent of the affected regions may be much broader than shown by individual spacecraft. Studies comparing satellite wave observations with Balloon Array for Radiation belt Relativistic Electron Losses (BARREL) data (Li et al., 2014) or examining correlations between ground magnetometer data and electron precipitation events observed in space by POES (Polar Orbiting Environmental Satellites) (Hendry et al., 2016) have shown large precipitation regions associated with EMIC waves. Although a variety of mechanisms can contribute to losses of radiation belt particles (e.g., Kim & Chan, 1997; Green et al., 2004; Millan & Thorne, 2007; Ni et al., 2013), the time scales for scattering by EMIC waves are short compared to the duration of a geomagnetic storm (e.g., Meredith et al., 2003). Thus, EMIC waves may be responsible for the electron flux drop-outs often observed at the beginning of the main phase of geomagnetic storms (e.g., Bortnik et al., 2006; Ukhorskiy et al., 2010; Sigsbee et al., 2016; Qin et al., 2019).

Ultra-low frequency (ULF) pulsations in the Pc1 band (0.5–5 Hz) (Jacobs et al., 1964) commonly observed in ground-based search coil magnetometer data are believed to be EMIC waves that have propagated from space to the ground. However, the extent of the regions in magnetic local time and latitude where EMIC waves are observed simultaneously in space and on the ground can be very different, due to wave generation processes and propagation effects, as well as the spatial coverage of the available data sets (e.g., Kim et al., 2011; Lessard et al., 2019; Sigsbee et al., 2020). Data from the Van Allen Probes have also shown that single spacecraft observations may underestimate the full extent of EMIC wave events in space (e.g., Blum et al., 2017). Due to the need to characterize the effects of EMIC waves on radiation belt and ring current dynamics and resolve differences in the observed spatial extents of EMIC waves on the ground and in space, many statistical studies of the spatial distributions of EMIC waves and their properties have been conducted using satellite data in the past 30 years (e.g., Anderson et al., 1992a, 1992b; Min et al., 2012; Usanova et al., 2012; Meredith et al., 2014).

Observations of EMIC waves often have interesting features related to propagation effects and the specific plasma conditions in the regions where the waves were generated. Examples of these structured EMIC waves include oxygen cyclotron harmonics (Usanova et al., 2016), regularly spaced series of repeating EMIC wave bursts known as Pc1 pearls, and intervals of alternating Poynting fluxes (Erlandson et al., 1992; Loto'ainu et al., 2009; Paulson et al., 2014, 2017; Usanova et al., 2008). In this paper, we will give special attention to EMIC waves with rising tones, which are sometimes referred to as triggered emissions in the literature, and have recently become of topic of interest due to increased availability of high time resolution magnetic field data from satellites in the relevant magnetospheric regions.

Pickett et al. (2010) was one of the first papers to examine spacecraft observations of EMIC triggered emissions as a separate phenomenon distinct from other types of wave structures found in the Pc1 frequency range. According to Pickett et al. (2010), examples of rising tone structures may have been included in earlier published studies (Mursula, 2007; Mursula et al., 1994) but they were not recognized as being a unique type of EMIC wave fine structure. In time-frequency power spectrograms of magnetic field data, EMIC rising tones or triggered emissions usually appear as discrete structures that rapidly increase in frequency, on time scales of several seconds up to about 1–2 min. The single event observed by the Cluster spacecraft near the nightside plasmopause on 30

March 2002 reported by Pickett et al. (2010) featured frequency-time dispersion similar to whistler mode chorus, with the starting frequencies located within the band of simultaneously observed EMIC waves, a high level of coherence, and Poynting flux propagation away from the equator. Chorus emissions (a few hundreds of Hz to several kHz) were named thusly because these radio waves sound like a “chorus” of birds chirping at dawn when they are played back as audio (Storey, 1953). Similarly, when the magnetic field waveforms of EMIC rising tones in the Pc1 frequency range (0.2–5 Hz) are time-compressed by a factor of about 300 to up-convert them into the audio frequency range, the chirp-like nature of these waves can also be clearly heard. Further studies of EMIC wave rising tones were conducted using Cluster data (Grison et al., 2013, 2016, 2018; He et al., 2014), but this mission's orbit may not have been ideal for studying these waves and very few cases were reported. Statistical studies of the occurrence rates of EMIC waves with rising tones have been performed using data from the Time History of Events and Macroscale Interactions during Substorms (THEMIS) mission (Nakamura et al., 2014, 2015, 2016).

EMIC waves with rising tones are a non-linear phenomenon, and development of theories to explain their generation has followed similar pathways to the development of non-linear models that simulate whistler mode chorus elements (e.g., Omura & Summers, 2006; Omura et al., 2010). Using the observations from Pickett et al. (2010), a mechanism was proposed for EMIC wave rising tone generation that invokes an initial period of linear wave amplitude growth followed by a nonlinear phase in which wave-particle interactions between the EMIC wave and resonant protons lead to an increase in the frequency of the emission (Omura et al., 2010). The triggering process for rising tones in this theory requires a dense plasma with a population of hot protons, such as a mixture of plasmaspheric and ring current particles. Hybrid simulations have been able to reproduce EMIC wave triggered emissions, and when the energetic proton density and the temperature anisotropy are high enough, the model can produce successive triggered emissions (Shoji & Omura, 2011). Theoretical studies predict EMIC wave rising tones may be observed in both the H⁺ and He⁺ bands, but triggering He⁺ band waves requires higher energy hot protons (Shoji & Omura, 2012). Later studies have also considered observations and theory of EMIC waves with falling tones (Shoji & Omura, 2017), sub-packet structures within individual rising tones (Nakamura et al., 2015; Shoji & Omura, 2013), and the formation of ion holes (Shoji et al., 2017). Modeling and theoretical studies indicate that EMIC rising tone emissions are very efficient at scattering radiation belt electrons (Kubota et al., 2015; Kubota & Omura, 2017) and energetic protons (Shoji & Omura, 2012; Shoji et al., 2011). Some work has also suggested that EMIC rising tone emissions could be related to structured Pc1 pulsations observed on the ground (Nakamura et al., 2014) and pulsating proton aurora (Nomura et al., 2016).

EMIC wave rising tones have been observed by the Van Allen Probes mission, but so far only a few case studies have been examined in detail (Engebretson et al., 2015; Nakamura et al., 2019; Sigsbee et al., 2020). Although there have been several statistical studies of EMIC waves using Van Allen Probes data (Chen et al., 2019; Jun et al., 2021; Saikin et al., 2015, 2016; Yu et al., 2015), these studies did not examine the occurrence rates of EMIC waves with rising tones. The study presented in this paper differs from the earlier statistical studies of EMIC waves observed by the Van Allen Probes in that we will consider both the occurrence rates of EMIC waves by frequency band and the occurrence rates of EMIC waves with rising tones over the time period 2012–2016. We will compare our overall occurrence rates for EMIC waves from the Van Allen Probes with past statistical studies and compare our occurrence rates for EMIC waves with rising tones to surveys of this phenomenon using data from THEMIS (e.g., Nakamura et al., 2016, 2015, 2014) and Cluster (Grison et al., 2013, 2018).

2. Data Coverage and EMIC Wave Event Selection

2.1. The Van Allen Probes EMFISIS Fluxgate Magnetometers

NASA launched the twin Radiation Belt Storm Probes (RBSP-A and RBSP-B) on 30 August 2012 to study how electromagnetic waves and other processes regulate the strength of the Earth's radiation belts. The mission was re-named in November 2012 to honor James Van Allen, the University of Iowa scientist who discovered the radiation belts in 1958. The two Van Allen Probes were in nearly identical orbits with $\sim 10^\circ$ inclinations and perigees and apogees of 1.1 and 5.8 R_E geocentric, respectively. The Electric and Magnetic Field Instrument Suite and Integrated Science (EMFISIS) instrument suite (Kletzing et al., 2013) tri-axial fluxgate magnetometers measured DC to ~ 30 Hz magnetic fields and provided coverage of the O⁺, He⁺, and H⁺ EMIC wave bands over most of the Van Allen Probes' orbits. We used data from September 2012 through the end of June 2016 to examine the occurrence rates of all EMIC waves and EMIC waves with rising tones for approximately two complete local time

Table 1
Van Allen Probes Data Quality and Availability 07 September 2012 to 01 July 2016

	RBSP-A	RBSP-B	Combined
Total minutes of orbital coverage	2005920.0	2005920.0	4011840.0
Minutes of orbital coverage with $L > 1.5$	1878632.0	1879753.0	3758385.0
Minutes of orbital coverage with $L > 1.5$ affected by:			
Thruster firings	13108.0	12420.0	25528.0
Data gaps	7418.0	3699.0	11117.0
High background levels	0.0	21262.0	21262.0
Total minutes of orbital coverage with $L > 1.5$ excluded	20526.0	37058.0	57584.0
Percentage of orbital coverage with $L > 1.5$ excluded	1.1%	2.0%	1.5%
Remaining minutes of orbital coverage with $L > 1.5$	1858106.0	1842695.0	3700801.0
Minutes of orbital coverage with EMIC waves	48908.0	39558.0	88466.0
Percentage of orbital coverage with EMIC waves	2.6%	2.1%	2.4%
Minutes of orbital coverage with rising tones	3471.0	3729.0	7200.0
Percentage of orbital coverage with rising tones	0.2%	0.2%	0.2%

precessions. We created statistical maps of the Van Allen Probes' orbital coverage and maps of the occurrence rates of all EMIC waves and EMIC waves with rising tones in bins of L shell and magnetic local time (MLT). We also made maps of the orbital coverage and occurrence rates in bins of R_{XY} and Z using the solar-magnetic (SM) coordinate system. In the following sections, we discuss how we selected EMIC wave events and show examples of EMIC waves with rising tones.

2.2. Spacecraft Interference and Excluded Time Intervals

All satellite scientific instruments can be affected by artificial signals produced by instrument electronics and other spacecraft systems. In most cases it was possible to work around these issues on the Van Allen Probes and our data analysis was unaffected. Minor issues in the calibrated fluxgate magnetometer data included a 14.5 Hz signal from an aliased heater line, a 1.5 Hz signal related to the SPICE (Spacecraft, Planet, Instrument, "C-matrix," Events) kernels, and an 11-s signal produced by the spacecraft spin period. These artificial signals were usually narrow-banded in frequency, relatively constant, and did not vary much over the spacecraft orbits. The 14.5 Hz signal due to the heater on RBSP-A was generally above the H⁺ cyclotron frequency, and did not affect EMIC wave identification. Due to the precision of the SPICE kernels that determine the attitude solution for de-spinning the fluxgate magnetometer data, when the Van Allen Probes were close to perigee the data often have interference lines at harmonics of the spacecraft spin period. These interference lines sometimes make it difficult to identify EMIC waves at low altitudes in the O⁺ and He⁺ bands. Increasing the fast Fourier transform (FFT) window size for the magnetic field spectrograms provides higher frequency resolution, which helps separate interference lines and EMIC waves, so that these signals did not cause issues with EMIC wave identification.

The Van Allen Probes fluxgate magnetometer had different gain settings to cover the expected magnetic field amplitude ranges. Nominally, the magnetometer operated in either Range-0 (0–256 nT, 0.001 nT resolution) or Range-1 (0–4,096 nT, 0.16 nT resolution). Each instrument count had 1/16 the amplitude resolution in Range-1 as it did in Range-0. The switch between Range-0 and Range-1 usually occurred between $L \sim 1.5$ and 2.0. We restricted our study to $L > 1.5$, as lower L shells could not be consistently screened for EMIC waves. The minimum L shell where EMIC waves were recorded was $L = 1.9$ on RBSP-A and $L = 1.8$ on RBSP-B.

Table 1 shows from September 2012 through June 2016, the Van Allen Probes spent a combined total of 4,011,840 min in orbit that could potentially be examined for EMIC waves. There were 3,758,385 min when the spacecraft were above $L = 1.5$, but not all of them could be properly screened for EMIC waves due to instrumental issues. When we binned the data by L and MLT or R_{XY} and Z SM, we determined the EMIC wave occurrence rates by dividing the number of minutes EMIC waves were observed in each position bin by the number of minutes of orbital coverage in that bin. Unusable time intervals had to be excluded in order to determine the correct

normalization factor for each position bin to avoid biasing the EMIC wave occurrence rates. Table 1 summarizes how many minutes of orbital coverage were excluded and what remained. In the following paragraphs, we discuss the reasons for excluding these time periods.

Thruster firings to maintain the spacecraft orbits produced distinctive signals in the FFT spectrograms of the fluxgate magnetometer data. Although strong EMIC waves sometimes can be observed above the background noise level during maneuvers, these data are not suitable for scientific use due to rapid changes in the spacecraft attitude. We excluded time intervals when spacecraft maneuvers were performed from the maps of orbital coverage and our data analysis because EMIC waves could not be accurately and consistently identified. As shown in Table 1, during the time period covered by our study 13,108 min of RBSP-A data and 12,420 min of RBSP-B data had to be eliminated due to spacecraft maneuvers.

Although the EMFISIS fluxgate magnetometers operated continuously throughout the Van Allen Probes mission, there were occasionally large gaps when the data were unrecoverable. Time intervals with data gaps >30 min were excluded from the maps of orbital coverage to avoid biasing the statistics. As shown in Table 1, during the time period covered by our study, 7,418 min of RBSP-A and 3,699 min of RBSP-B orbital coverage were unrecoverable and had long data gaps.

Some unique issues only affected RBSP-B. On 9 October 2015, a single event upset on RBSP-B triggered a contingency mode which required a processor reset on 13 October 2015 to resume normal operations. During this time the RBSP-B fluxgate magnetometer was forced into Range-3 (0–65,000 nT, 2 nT resolution). The increase in the background noise level and degraded amplitude resolution in Range-3 could not be corrected. Although EMIC waves were sometimes visible in the RBSP-B spectrograms from this time, we excluded orbits 3019–3030 from our coverage map and EMIC wave event list due to the loss of amplitude resolution.

Although the RBSP-A and RBSP-B fluxgate magnetometers were identical, RBSP-B was affected by unknown sources of interference during the early part of the mission that occasionally caused higher background noise levels than on RBSP-A. We chose a minimum power spectral density threshold of 10^{-3} nT²/Hz for EMIC wave observations, but background signal levels on RBSP-B sometimes exceeded this threshold. For comparison, on RBSP-A the background noise level in the power spectral density usually varied between 10^{-5} and 5×10^{-4} nT²/Hz when the instrument was in Range-0. The unknown interference in the RBSP-B fluxgate magnetometer data could persist for several consecutive orbits. It was not related to spacecraft maneuvers or the artificial signals discussed above, and did not appear to be associated with known spacecraft charging events or eclipse periods. The high background levels on RBSP-B sometimes appeared to be related to the heater, but this does not fully explain all cases, and the cause remains unknown.

For most affected RBSP-B orbits, the background noise level in the power spectral density was below 10^{-4} to 10^{-3} nT²/Hz. Adjusting the lower color bar range from 10^{-5} to 10^{-4} nT²/Hz on the survey spectrograms usually cut out most of the interference, and it was possible to identify EMIC waves with amplitudes above 10^{-3} nT²/Hz. Unfortunately, a number of RBSP-B orbits in February and March 2013 had interference at levels greater than 10^{-2} nT²/Hz over the entire frequency range of interest. When the background noise levels from 0.12 to 10 Hz on RBSP-B was greater than 10^{-2} nT²/Hz in B_x and/or B_y SM over 50% or more of an orbit, we excluded the affected time intervals because EMIC waves could not be consistently identified. Table 1 shows that 21,262 min of data were excluded due to the Range-3 issue for RBSP-B orbits 3019–3030 and intervals with high background levels on RBSP-B. After August 2013 (around orbit 900), the fluxgate magnetometer background levels on most RBSP-B orbits were comparable to those on RBSP-A. Thus, there are gaps in the RBSP-B coverage early in the mission, and some low amplitude EMIC waves may have been missed.

Overall, 20,526 min of data when RBSP-A was at $L > 1.5$ and 37,058 min of data when RBSP-B was at $L > 1.5$ were excluded from our study due to various issues. This represents only 1.1% of the total RBSP-A orbital coverage for $L > 1.5$ and 2.0% of the total RBSP-B orbital coverage for $L > 1.5$. Note that the sum of the minutes of orbital coverage affected by thruster firings, data gaps, and high background levels in Table 1 is greater than the total number of minutes of orbital coverage we excluded for RBSP-B, as some of the time periods affected by high background levels were also affected by thruster firings. After accounting for data gaps and excluding intervals with other issues, we had 1,858,106 min of data from RBSP-A and 1,842,695 min of data from RBSP-B that could be screened for EMIC waves.

2.3. EMIC Wave Identification and Rising Tone Examples

We identified EMIC waves using Autoplot (Faden et al., 2010), an open-source interactive data browser developed under the NASA Virtual Observatories for Heliophysics Program. Autoplot allows quick and interactive browsing of data and metadata files found on the Internet, such as NASA Common Data Format (CDF) or ASCII files. Autoplot has built-in features to aid in navigating very large data sets, such as a PNGWalk tool which creates sequences of standardized Portable Network Graphics (PNG) survey plot images that can be viewed on a timeline. With a single button click, the Autoplot PNGWalk tool can use a survey plot to load the corresponding full resolution data sets from the original CDF files into an interactive plot window. The Autoplot PNGWalk tool also has a quality control utility that can be used to flag time intervals with issues, such as the data gaps mentioned in the previous section. Autoplot supports scripting in Jython, the Java-based implementation of Python, to allow users to add their own customized data analysis operations, such as overplotting key plasma wave frequencies on a spectrogram or digitizing data.

To aid in navigating the Van Allen Probes data, we generated a set of Autoplot PNGWalk images of the EMFISIS fluxgate magnetometer data from 7 September 2012 (RBSP-A Orbit 24 and RBSP-B Orbit 24) through 1 July 2016 (RBSP-A Orbit 3750 and RBSP-B Orbit 3723). This date range provided coverage of the full range of magnetic local times twice. We used the set of PNGWalk images to track our progress and flag orbits with potential issues. We used Jython scripts to create a customized digitization tool to save the start and end times of each interval of EMIC waves, record the frequency band (H+, He+, or O+), and note whether or not rising tones were observed. The digitization tool used the set of PNGWalk images to load single orbits of data from the original, full-resolution EMFISIS fluxgate magnetometer CDF files into an Autoplot interactive plot window. The digitization tool worked from FFT spectrograms of the 64 samples/s EMFISIS fluxgate magnetometer B_x and B_y in SM coordinates. In the solar-magnetic (SM) coordinate system, the Z axis is along the Earth's magnetic dipole axis, and the X-Y plane is perpendicular to the Earth's dipole axis. The B_x and B_y components in SM coordinates were chosen because EMIC waves propagate primarily along the background magnetic field with transverse wave magnetic field fluctuations that are mainly perpendicular to the background magnetic field. In contrast, magnetosonic waves typically propagate close to the magnetic equator in both the radial and azimuthal direction, with wave magnetic field fluctuations along the background magnetic field, and thus would appear in the B_z SM component of the magnetic field. Because EMIC waves are transverse waves, not compressional waves, they will not appear very strongly in the total magnetic field, if they even appear in B total at all.

Our digitization tool allowed us to adjust the FFT size, time and frequency scales, and color bar for the spectrograms in the interactive plot window as needed to mark each interval of EMIC waves. The initial spectrograms loaded by the digitization tool showed a single orbit of data starting at one perigee and ending at the next perigee. The H+, He+, and O+ ion gyrofrequencies calculated using the total magnetic field measured by EMFISIS were overplotted on the spectrograms using another Jython script to aid in identifying the three main EMIC wave bands. The initial spectrograms loaded by the digitization tool used a 1024-point sliding Hanning window with 3/4 overlap between windows, which is usually adequate for identifying H+ and He+ band EMIC wave rising tones in the Van Allen Probes data set. For 64 samples/s data, a 1024-point FFT window corresponds to a 16 s window that slides over by 4 s. The shortest time-scale structure that can be resolved using this FFT window is about 8–12 s, which corresponds to two or three overlapping windows. A 512-point FFT would allow features on shorter time scales to be identified, but provides coarser frequency resolution. Due to variations in the observed local ion gyrofrequencies, sometimes a 2048-point FFT was needed to identify He+ band EMIC waves, and a 4096-point FFT was needed for O+ band EMIC waves.

Using the digitization tool, we marked each interval of EMIC waves on either the B_x or B_y SM spectrogram. The digitization tool drew color-coded bars on top of the spectrograms to indicate which intervals of EMIC wave activity had already been recorded. For this task, we required EMIC waves to have minimum power spectral densities of $\sim 10^{-3}$ nT²/Hz in either the B_x or B_y SM spectrogram and to be visible above the background noise level of the spectrogram. A single interval of EMIC wave activity could have variations in power spectral density as long as it did not drop below 10^{-3} nT²/Hz. Likewise, a highly variable EMIC wave event lasting several hours could have multiple intervals of EMIC wave activity if the power spectral density fluctuated and fell below 10^{-3} nT²/Hz. Digitizing EMIC wave intervals from the spectrograms was time-consuming, but generally a straightforward process. However, some care needed to be exercised to avoid other types of waves that could be found in similar frequency ranges. Broadband ultra-low frequency (ULF) waves or Pc5 field line resonances

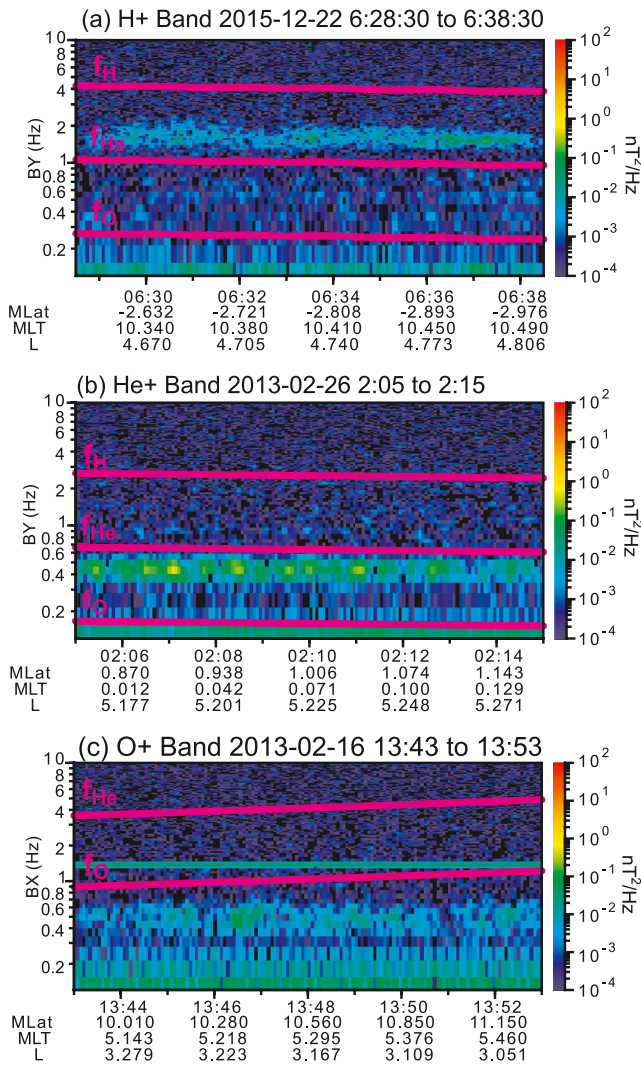


Figure 1. Example 10-min spectrograms of either the B_Y or B_X SM component of the magnetic field from RBSP-A showing (a) EMIC waves from the proton (H+) band, (b) the helium (He+) band, and (c) the oxygen (O+) band. The H+, He+, and O+ ion gyrofrequencies (f_H , f_{He} , and f_O) are marked with magenta lines.

harmonics are also observed by the Van Allen Probes, but these waves are usually found far below the O+ cyclotron frequency and are distinct from O+ band EMIC waves. In a few cases, we performed wave normal analysis (Santolík et al., 2003) to aid in proper wave identification. On average, each orbit with EMIC waves had 3 to 4 separate intervals of wave activity. We identified 976 RBSP-A orbits and 857 RBSP-B orbits with EMIC waves from September 2012 through the end of June 2016.

In FFT time-frequency spectrograms of the magnetic field power spectral density, EMIC waves observed in space usually appear as a narrow band of wave power within the broader bands delineated by the gyrofrequencies of the major magnetospheric ion species H+, He+, and O+. The exact wave cutoff frequencies within these bands depend upon the relative concentrations of the different ion species (e.g., Min et al., 2015). Because the ion gyrofrequencies depend upon the background magnetic field strength, which varies with distance from the Earth, the frequencies of EMIC waves in space vary slowly along the observing satellite's orbit. Temporal changes in the Earth's magnetic field due to geomagnetic disturbances associated with interplanetary shocks, geomagnetic storms, and particle injections can produce variations in the wave frequencies on time scales of a few minutes to a few hours. The examples of EMIC waves in Figures 1–3 all show only 10 min of data from time intervals when the background magnetic field was relatively stable to make it easier to see the difference between an unstructured EMIC wave and what we classified as EMIC waves with rising tones in our study.

Figure 1 shows example spectrograms of either the B_X or B_Y SM component of the magnetic field from RBSP-A for EMIC waves in (a) the proton (H+) band from 22 December 2015 (centered around ~ 1.5 Hz), (b) the helium (He+) band from 19 February 2012 (centered around ~ 0.45 Hz), and (c) the oxygen (O+) band from 16 February 2013 (centered around ~ 0.5 Hz). The H+, He+, and O+ ion gyrofrequencies (f_H , f_{He} , and f_O) are marked with magenta lines. These examples were made using a 1024-point FFT window with $\frac{3}{4}$ overlap. The frequency range of the EMIC wave examples is 0.12–10 Hz to avoid the spacecraft spin tone. The constant frequency tone in Figure 1c near 1.5 Hz is one of the instrumental interference lines mentioned in Section 2.2. The EMIC waves from each band shown in Figure 1 are clearly bounded by the ion gyrofrequencies. Although the wave power varies slightly throughout the time intervals shown, these waves do not have rising tones. The small variations in the wave frequencies across each 10-min example are mainly due to changes in the ion gyrofrequencies along the Van Allen Probes' orbits.

Figure 2 shows 10-min example spectrograms of either the B_X or B_Y SM component of the RBSP-A magnetic field for short (<10 min duration) bursts of EMIC waves with rising tones. The rising tones are indicated by black arrows. In the H+ EMIC wave band, the rising tones appear as intense peaks in the magnetic field power spectral density that rise upwards in frequency out of the main band of EMIC waves. The magnetic field waveform for an EMIC wave rising tone would show a chirp-like structure of sinusoidal oscillations that increase in frequency contained within the envelope of well-defined wave packet (e.g. Shoji & Omura, 2013). The interval of unstructured H+ band EMIC waves shown in Figure 1a and the rising tone example in Figure 2a are both from the 22 December 2015 scattering event studied in Sigsbee et al. (2020). Figures 1a and 2a illustrate how intervals of unstructured EMIC waves and waves with rising tones can be found along the same Van Allen Probes orbit, within just a few minutes of one another. Many short intervals of EMIC waves like those shown in Figure 2 only have a few rising tones. Figure 3 has a similar format to Figures 1 and 2, and shows examples of (a) and (b) two 10-min intervals of H+ band waves with rising tones and (c) an example of He+ band waves with rising tones that are part of much longer duration (>10 min) intervals of wave activity. The examples in Figures 3a and 3b are from an EMIC wave event on 23 February 2014 that was several hours in duration and occurred over a broad range of local times (Engebretson et al., 2015). While

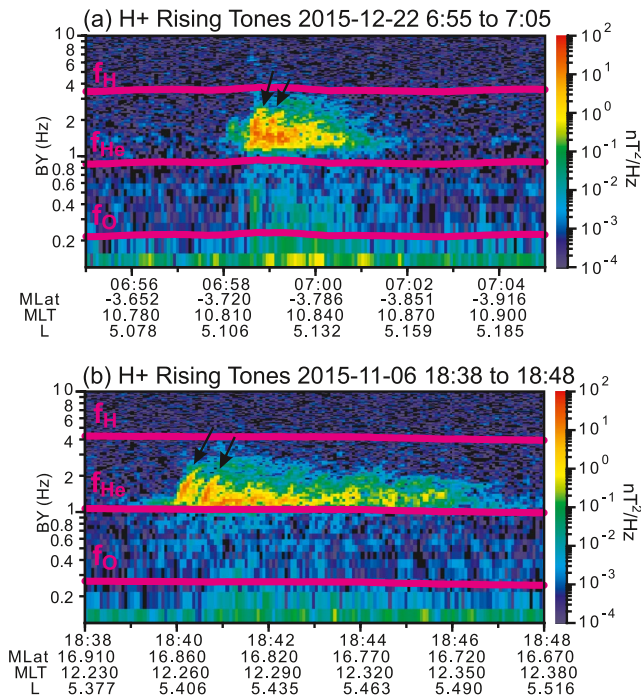


Figure 2. Spectrograms of B_y , SM showing short <10 min bursts of H+ band EMIC waves with rising tones from RBSP-A on (a) 22 December 2015 and (b) 6 November 2015 in a similar format to Figure 1.

longer intervals of EMIC waves like those shown in Figure 3 may have many rising tones, it is important to note that the intervals of EMIC wave activity we marked as having rising tones during the digitization process have variable time durations, variable numbers of rising tone elements, and may also have long periods of unstructured EMIC waves.

The examples shown in Figures 2 and 3 are similar to the H+ rising tones observed on Cluster (Grison et al., 2013; Pickett et al., 2010) and He+ rising tones observed by THEMIS (Nakamura et al., 2014). EMIC rising tones observed by Cluster had variable frequency sweep rates with some examples changing in frequency by about 1.5 Hz over 50 s (He et al., 2014) and others having frequency changes of ~ 0.5 – 1.9 Hz and durations of ~ 44 – 62 s (Grison et al., 2013). In Figures 2 and 3, the H+ band EMIC wave rising tones stand out from the lower-amplitude band of unstructured EMIC waves as large-amplitude features that change in frequency by 0.3 – 1.3 Hz over 14 – 56 s, and have positive slopes $\Delta f/\Delta t$ in the range 1.6×10^{-2} – 5.2×10^{-2} Hz/s as measured from either the B_x or B_y spectrograms. For the He+ rising tones in Figure 2c from 21:36–21:46 UT on 25 July 2013, Δf ranged from 0.29 to 0.39 Hz and Δt ranged from 32 to 57 s, for slopes $\Delta f/\Delta t$ in the range 6.2×10^{-3} to 1.1×10^{-2} Hz/s as measured from the B_x spectrogram. Because the sweep rates are quite variable, we did not place any requirements on $\Delta f/\Delta t$ in order to mark an interval as having rising tones. Our key requirement was only that the structure clearly stand out from the background on the spectrogram and have a positive slope, as in the examples shown. There have also been reports of EMIC wave falling tones (Nakamura et al., 2016; Shoji & Omura, 2017), but they will not be considered by our study. We did not find many clear cases during our survey and falling tones appear to be rare in the

Van Allen Probe data set. We also will not examine the occurrence of other EMIC wave fine structures such as Pc1 pearls (Paulson et al., 2017) and harmonics (Usanova et al., 2016) in this paper, and did not place waves with such structures into separate categories. We will only compare the occurrence rates for EMIC waves with rising tones to the occurrence rates of all EMIC waves.

3. Occurrence Rates for EMIC Waves

In addition to showing the minutes of orbital coverage available for our study, Table 1 also shows the number of minutes of orbital coverage that had EMIC waves and EMIC waves with rising tones. EMIC waves were observed about 2.6% of the of time when RBSP-A was at $L > 1.5$, and 2.1% of the time when RBSP-B was at $L > 1.5$. When both spacecraft are considered together, EMIC waves were observed about 2.4% of the time. EMIC waves with rising tones were only observed about 0.2% of the time on both spacecraft.

The overall occurrence rates of each EMIC wave band observed by both RBSP-A and RBSP-B combined from September 2012 through June 2016 are presented in Table 2 with standard errors (Bevington & Robinson, 2003). The Saikin et al. (2015) study included data from the first 22 months of the Van Allen Probes mission, from 8 September 2012 to 30 June 2014, and found 452.96 hr of EMIC waves combined in all three bands. As shown in Table 2, we found a total of 101,418 min, or 1,690 hr, of EMIC waves in all three bands through the end of June 2016. Saikin et al. (2015) found 35% of EMIC waves were in the H+ band, 59% were in the He+ band, and 7% were in the O+ band. Although we covered a different time period and used slightly different selection conditions from Saikin et al. (2015), the breakdowns of EMIC waves by frequency band shown in Table 2 compare favorably to the earlier study.

The overall counts for all EMIC waves in Table 1 only indicate waves were observed during a given minute of orbital coverage, and do not take into account that more than one band of EMIC waves could have been observed simultaneously. Thus, the total number of minutes of orbital coverage when EMIC waves were observed in Table 1 does not equal the sum of the minutes when each individual EMIC wave band was observed in Table 2. For both RBSP-A and RBSP-B combined, the difference implies there were 12,952 min of data when more

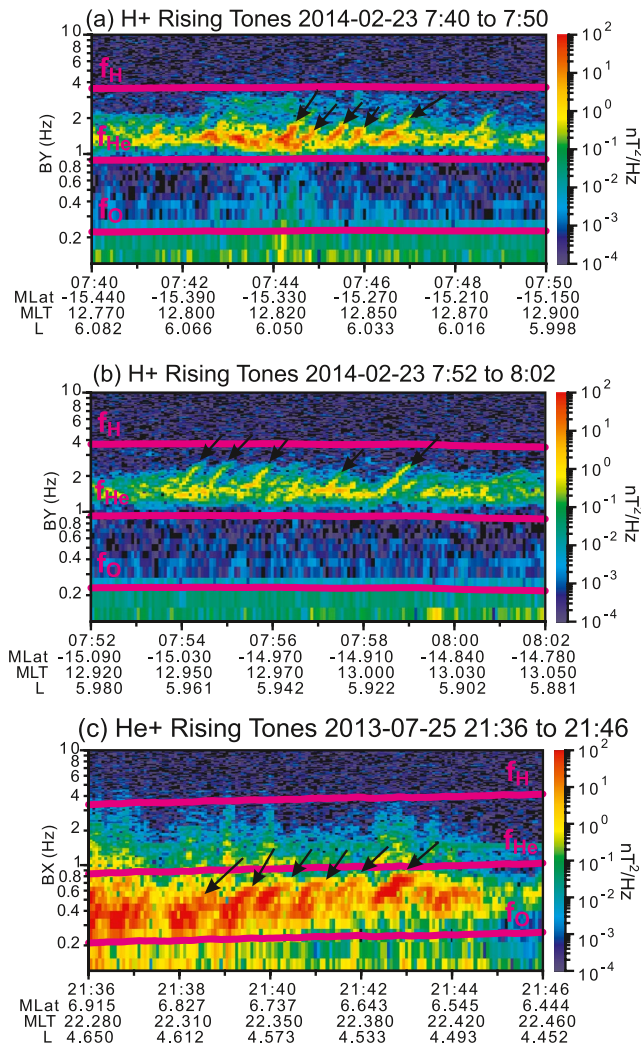


Figure 3. 10-minute spectrograms of RBSP-A data showing portions of much longer EMIC wave events on 23 February 2014 with (a and b) H+ band rising tones, and (c) on 25 July 2013 with He+ band rising tones in a similar format to Figure 1.

than one band of EMIC waves was observed. Although multi-banded events constitute a considerable amount of data, the majority of EMIC wave events appear to have consisted of a single band.

Table 3 shows the occurrence rates for EMIC waves with rising tones in the H+ and He+ bands for both RBSP-A and RBSP-B combined together. No EMIC waves with rising tones were found in the O+ band. Overall, 91.8% of H+ band EMIC waves did not have rising tones and 92.9% of He+ band EMIC waves did not have rising tones. Only 8.2% of H+ band EMIC waves had rising tones, and only 7.1% of He+ band EMIC waves had rising tones. The pie charts in Figure 4 provide a graphical summary of the occurrence statistics from Tables 2 and 3.

4. EMIC Wave Occurrence as a Function of L and MLT

To examine the spatial distributions of EMIC waves, we organized the Van Allen Probes orbital coverage and the digitized EMIC wave intervals into 1-hr bins of MLT and 0.5 bins of L shell. L shells were generated using the Van Allen Probes SPICE kernels and based upon the SM geomagnetic latitude calculated from the IGRF (International Geomagnetic Reference Field) model. The ratio R/L is very close to 1 over the entire range of magnetic latitudes and radial distances covered by the Van Allen Probes. L and R differ by less than 1% near the equator and by no more than 10%–12% at the highest latitudes covered. To determine the percentage of time EMIC waves were observed, we divided the number of minutes of EMIC waves observed in each bin by the number of minutes the spacecraft spent in that bin. The top panel of Figure 5 shows the percentage of time EMIC waves in any band were observed by both of the Van Allen Probes combined in each bin of L and MLT. The bottom panel of Figure 5 shows the minutes of orbital coverage in the same bins of L and MLT for both of the Van Allen Probes combined. Figure 5 shows slightly enhanced EMIC wave occurrence rates between 9 MLT and noon between $4 < L < 6$. The peak EMIC wave occurrence rates were found between noon and 18 MLT, with the peak covering the broadest range of L shells around 15 MLT. Figure 6 shows maps of the EMIC wave occurrence rates as a function of L and MLT for both RBSP-A and RBSP-B combined in the same bins of L and MLT used in Figure 5 for each EMIC wave band. The top row of Figure 6 shows the occurrence rates for all H+ EMIC waves and only H+ EMIC waves with rising tones. The second row shows the occurrence rates for all He+ EMIC waves and only He+ EMIC

waves with rising tones. The bottom row shows the occurrence rates for O+ EMIC waves. We did not observe rising tones in the O+ band.

Figure 6 shows that the dayside was the preferred region for all H+ band EMIC waves, although H+ band waves were observed at all local times and over the entire range of L shells covered. Enhanced occurrence rates were found from 9 to 18 MLT, with the highest H+ band wave occurrence rates found between 11 and 16 MLT for $4 < L < 6.5$. Figure 6 shows that across the entire nightside region, the occurrence rates for all He+ band waves are about twice the occurrence rates for all H+ band waves. The regions with the lowest occurrence rates for all He+ band waves were all MLT for $L < 3$ and the dawn sector from 4 to 8 MLT for $L > 5$. The peak occurrence region for all He+ band waves was between noon and 18 MLT. There are two distinct regions of high O+ band occurrence rates. As shown in Figure 6, one region is located between $2 < L < 4$, from 3 MLT all the way around the dayside to 21 MLT. The second region of high O+ band occurrence rates was found at $L > 4$ on the dusk side from 15 to 20 MLT. The regions of high O+ EMIC

Table 2
Combined Minutes of EMIC Waves Observed From September 2012 Through June 2016

Total minutes of EMIC waves observed $n = 101418.0$ $\sigma = 318.5$			
Frequency band	n (minutes)	$\sigma = \sqrt{n}$	% of total minutes
H+	40,888.0	202.2	40.3 ± 0.2
He+	54,251.0	232.9	53.5 ± 0.3
O+	6,279.0	79.2	6.2 ± 0.1

Table 3
Combined Minutes of H+ and He+ EMIC Waves With Rising Tones

Type	H+			He+		
	$n = 40888.0$	$\sigma = \sqrt{n}$	%	$n = 54251.0$	$\sigma = \sqrt{n}$	%
No rising tones	37,545.0	193.8	91.8 ± 0.7	50,394.0	224.5	92.9 ± 0.8
With rising tones	3,343.0	57.8	8.2 ± 0.1	3,857.0	62.1	7.1 ± 0.1

wave occurrence may be the result of variations in plasma composition throughout the inner magnetosphere. The region of high O+ band occurrence at large L shells near dusk corresponds to where plasmaspheric plumes are likely to be found. The region of high O+ band occurrence over a broad range of magnetic local times at lower L shells corresponds to the region near the plasmopause.

The main objective of this study was to compare the occurrence rates of EMIC waves with rising tones to the overall occurrence rates for EMIC waves. Although H+ band EMIC waves in general were observed at all magnetic local times and over the full range of L shells covered by this study, Figure 6 shows that H+ band waves with rising tones were mainly found for $L > 4$. The region of peak occurrence for H+ band waves with rising tones is very similar to the region where H+ band waves were more likely to occur overall. While the Van Allen Probes did observe enough H+ band EMIC waves in general from midnight to 6 MLT to completely fill in the map, there were very few H+ band waves with rising tones found in this MLT region.

The regions where He+ band EMIC waves with rising tones were observed were also much more limited than for all He+ band waves. The map of the occurrence rates for He+ band waves with rising tones in Figure 6 shows these waves were most likely to be observed from 8 MLT around the dayside through the dusk sector, with a peak in the afternoon from 12 to 18 MLT. This broad region of the dayside is similar to where enhanced occurrence rates for all He+ waves were found. The occurrence rates for He+ waves with rising tones in the afternoon sector were relatively high compared to the occurrence rates for H+ band waves with rising tones in this region. It is interesting to note that although the occurrence rates for all He+ band waves were higher than those for all H+ band waves on the nightside, the occurrence rates for He+ band waves with rising tones were quite low in this region. Very few EMIC wave events with rising tones were found in either the H+ or He+ band on the nightside.

5. EMIC Wave Occurrence as a Function of R_{XY} and Z SM

Since the Van Allen Probes covered $\pm 20^\circ$ magnetic latitude, we examined how EMIC wave occurrence rates depended on the radial distance R_{XY} in the X-Y SM plane and the distance Z SM above the plane of the magnetic equator. We organized the orbital coverage and minutes of EMIC waves observed by both spacecraft into bins of $0.5 R_E$ in R_{XY} and bins of $0.25 R_E$ in Z SM. As before, we determined occurrence rates by dividing the minutes of EMIC wave observations by the time the spacecraft spent in each bin. We split the data into four magnetic local time sectors: midnight (21–3 MLT), dawn (3–9 MLT), noon (9–15 MLT), and dusk (15–21 MLT). Figure 7 shows

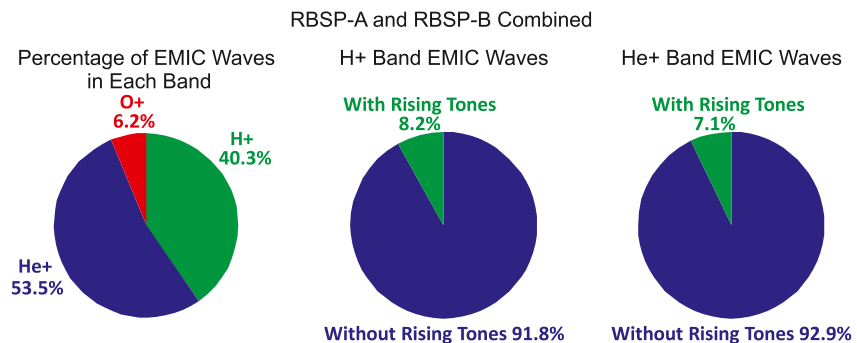
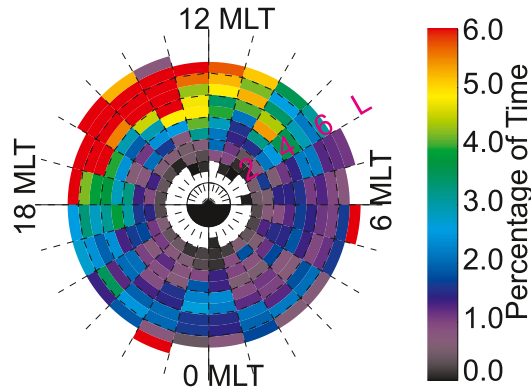


Figure 4. Pie charts for both spacecraft combined showing (a) the overall percentages of EMIC waves in the H+, He+, and O+ bands, (b) the percentages of H+ band waves with and without rising tones, (c) the percentages of He+ band waves with and without rising tones.

RBSP-A and RBSP-B Combined
Percentage of Time All Bands of EMIC Waves
Observed 2012-09-07 to 2016-07-01



Minutes of Orbital Coverage
2012-09-07 to 2016-07-01

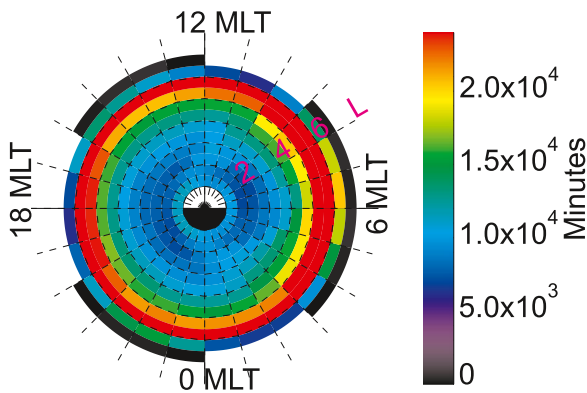


Figure 5. The overall percentage of time EMIC waves were observed by both spacecraft combined in bins of 0.5 L shell and 1 hr MLT, along with the Van Allen Probes orbital coverage in the same bins of L shell and MLT.

the combined minutes of orbital coverage for both RBSP-A and RBSP-B as functions of R_{XY} and Z SM in the four local time sectors. For reference, we plotted lines of constant SM latitude, and curves representing dipole L shells in Figure 7. The orbital coverage above and below the equatorial plane was mostly uniform, except for $4 < R_{XY} < 6 R_E$. The midnight, dawn, and dusk sectors in this R_{XY} range have slightly more coverage for negative latitudes, while the dusk sector has slightly more coverage for positive latitudes. This likely did not affect our results for the overall EMIC wave occurrence rates due to the large number of observations. However, the orbital coverage could have affected the results for the occurrence rates of H+ and He+ band waves with rising tones due to the smaller number of observations.

Figure 8 shows the occurrence rates for all EMIC waves observed by both spacecraft combined in the four local time sectors as a function of R_{XY} and Z SM. Overall, we found 85% of the EMIC wave events included in our study were observed by the Van Allen Probes between $\pm 15^\circ$ magnetic latitude. In the midnight sector, EMIC waves were somewhat uniformly distributed in Z SM, with peak occurrence rates near the equatorial plane between $4 < R_{XY} < 6 R_E$. In the dawn sector, there is a peak near the equator between $4 < R_{XY} < 6 R_E$, but there are also peaks around Z SM = $-1.5 R_E$ for $3.5 < R_{XY} < 5 R_E$, and above 10° latitude near apogee. Figure 8 shows most EMIC waves were found in the noon and dusk sectors, consistent with the L -MLT maps in Figures 5 and 6. Near noon, there is a peak in the occurrence rates for all EMIC waves from $-1 < Z$ SM $< 2 R_E$ (-10° to $+20^\circ$ latitude) between $4 < R_{XY} < 6 R_E$. This could be due to the effects of magnetospheric compressions, which are one source of ion anisotropy to drive EMIC waves on the dayside. In the dusk sector, the greatest occurrence of EMIC waves was found for $R_{XY} > 5 R_E$ and for Z SM > 0 , which may also be related to magnetospheric compressions. Near dusk, plasmaspheric drainage plumes may also impact the latitude range where enhanced EMIC wave occurrence rates were found. Recently, there have been reports of low-frequency magnetosonic waves below the proton gyrofrequency. Teng et al. (2019) examined the occurrence rates of these events using Van Allen Probes data from October 2012 to December 2018. The low-frequency magnetosonic waves were mainly observed inside the plasmasphere from the prenoon to the midnight sector within $\pm 5^\circ$ of the geomagnetic equator. This is quite different from Figure 8, which shows EMIC wave observations spread over $\pm 20^\circ$ MLAT with more high-latitude waves near noon and dusk at the largest radial distances.

Figure 9 is in the same format as Figure 8, but for all H+ band waves. Although the occurrence rates for all H+ band waves were low in the midnight sector, Figure 9 shows there was a slightly higher chance of observing H+ band waves between $4 < R_{XY} < 6 R_E$ near the equatorial plane. In the dawn sector, occurrence rates for all H+ band waves were higher than near midnight. H+ band waves are the source of the peak above 10° latitude near apogee for the overall distribution of EMIC waves near dawn in Figure 8. In the noon sector, the occurrence rates for H+ band waves have a peak between $4 < R_{XY} < 6 R_E$ and Z SM $> 0 R_E$. Near dusk, the occurrence rates for all H+ band waves are about twice the occurrence rates near dawn, as indicated by the color bar range in Figure 9. The L -MLT map of all H+ band EMIC wave occurrence rates in Figure 6 seems to have a slightly stronger peak near dusk than the map of the occurrence rates as a function of R_{XY} and Z SM in Figure 9. However, the L -MLT map projects all observations down into the equatorial plane, while the R_{XY} and Z SM map spreads the observations over latitude.

Figure 10 is in the same format as Figure 8, but for all He+ band waves. The peak for all He+ band waves in the midnight sector near the equator between $4 < R_{XY} < 6 R_E$ is similar to the peak in the midnight sector for all EMIC waves in Figure 8. Although the He+ band waves in the dawn sector are spread over a range of latitudes and radial distances, there are also a few localized peaks between $4 < R_{XY} < 5 R_E$. Most notably, there is a peak near Z SM = $-1 R_E$ corresponding to the peak in Figure 8 in the dawn sector for all EMIC waves. Figure 10 shows the highest occurrence rates for all He+ band waves in the noon sector are found from $4 < R_{XY} < 6 R_E$

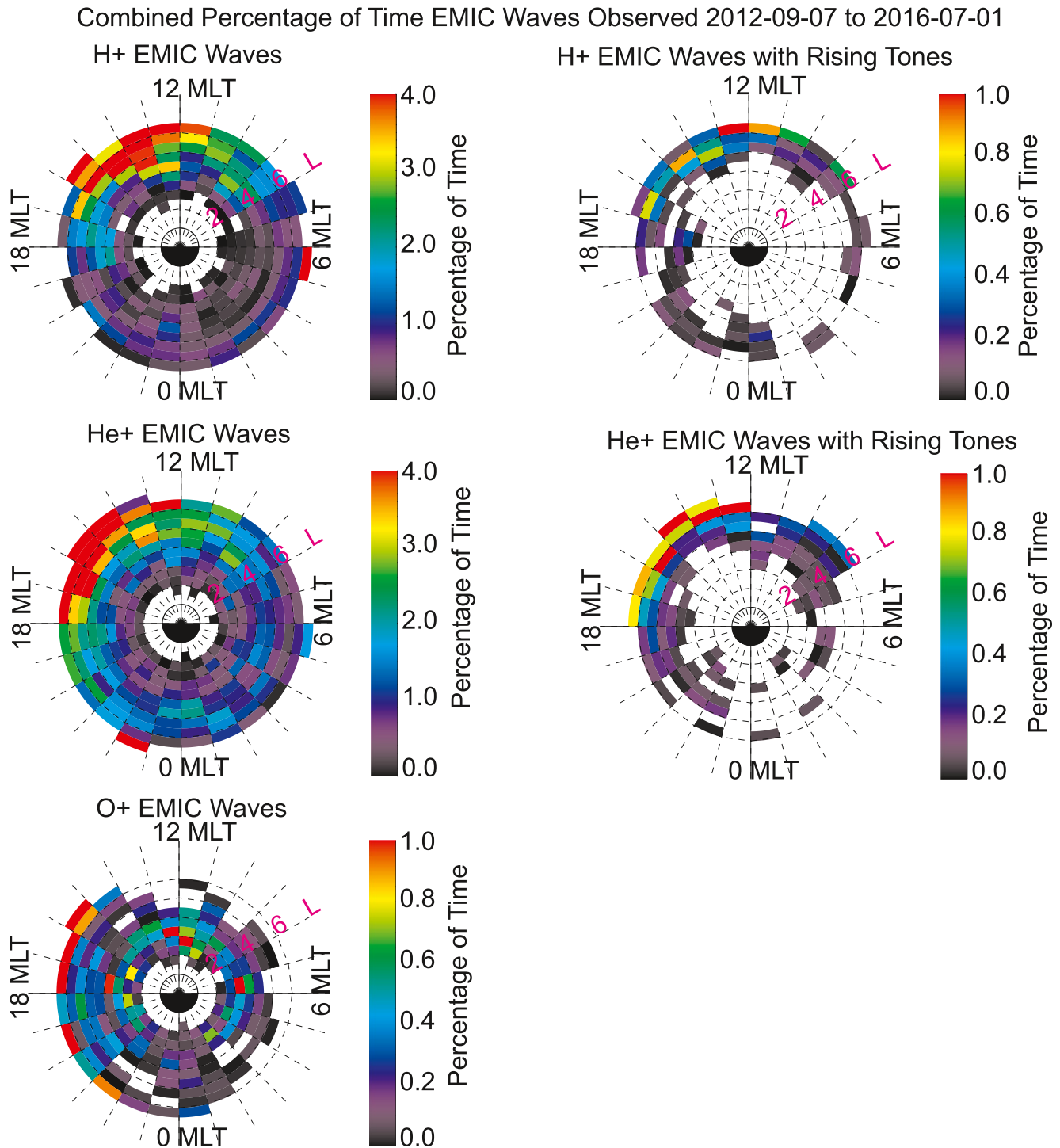


Figure 6. Occurrence rates for each EMIC wave band in the same L shell and MLT bins as Figure 5. First row: the percentage of time all H+ band EMIC waves were observed compared to the percentage of time H+ band EMIC waves with rising tones were observed. Second row: the percentage of time all He+ band EMIC waves were observed compared to the percentage of time He+ band EMIC waves with rising tones were observed. Third row: the percentage of time O+ band EMIC waves were observed. No rising tones were found in the O+ band.

and $+1 < Z \text{ SM} < +2 R_E$. In the dusk sector, there is an even stronger peak in the occurrence rates at the highest latitudes covered for $R_{XY} > 4 R_E$. It is also interesting that in the dusk sector there are relatively low occurrence rates compared to the other local time sectors for He+ band waves at latitudes between -10° and -20° for $R_{XY} < 4 R_E$. Comparisons between Figures 8–10 seem to show greater overall EMIC wave occurrence in the northern

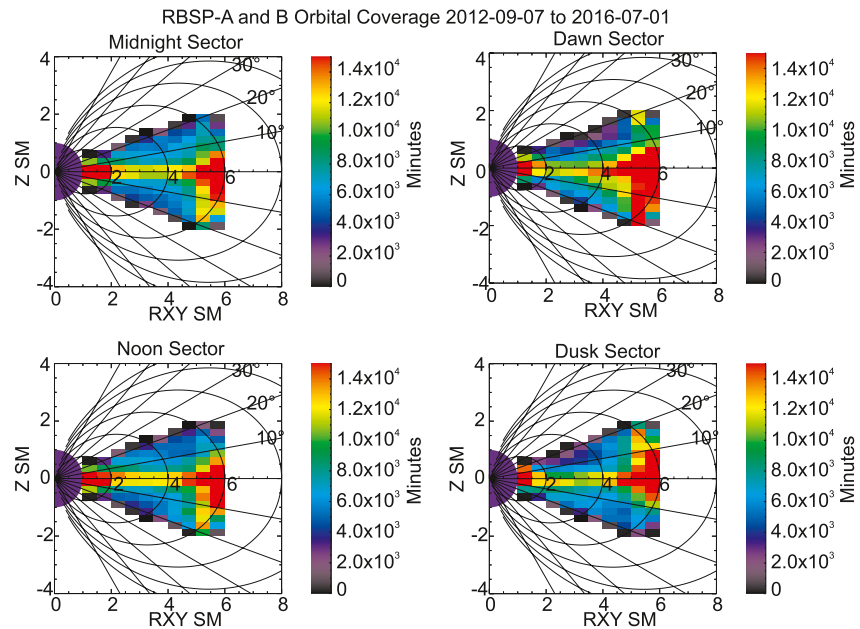


Figure 7. The number of minutes spent by the Van Allen Probes from 2012 to 2016 in four local time sectors as a function of $0.5 R_E$ bins of R_{XY} SM and $0.25 R_E$ bins of the Z SM location. Black lines indicate constant dipole magnetic latitude and L shells.

hemisphere for the noon sector (a combination of H⁺ and He⁺ band waves) and dusk sector (mostly He⁺ band waves). However, in Figure 7, it appears that there was slightly more orbital coverage of the northern hemisphere in the midnight, dawn, and noon sectors, while only the dusk sector had slightly more coverage in the southern hemisphere. It seems likely that the plots in Figures 8–10 showing EMIC waves were observed more frequently in the northern hemisphere result from a combination of the orbital coverage, seasonal effects due to when the northern hemisphere was covered in each local time sectors, and the geomagnetic activity during these times.

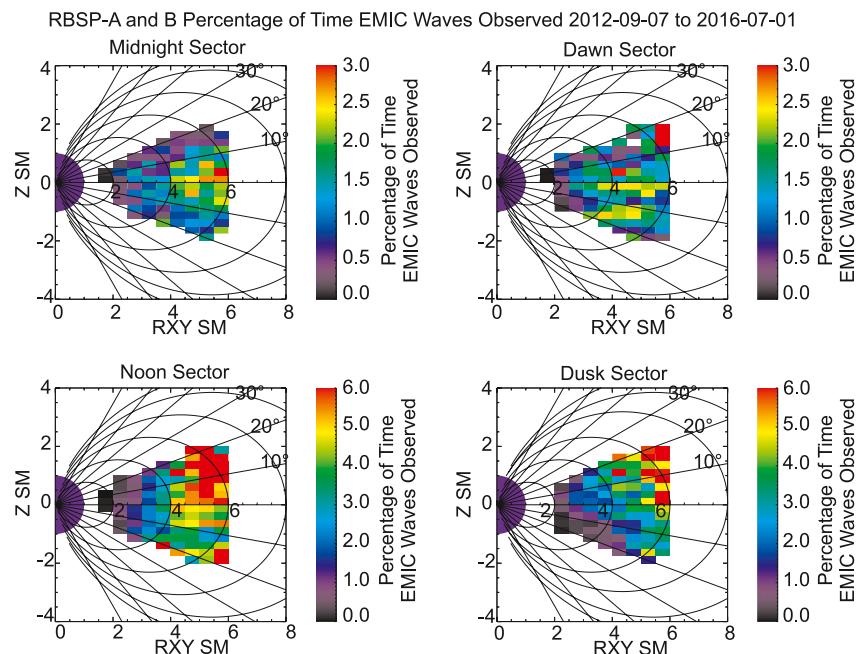


Figure 8. The overall occurrence rates of all EMIC waves observed by the Van Allen Probes in four local time sectors as a function of $0.5 R_E$ bins of R_{XY} SM and $0.25 R_E$ bins of the Z SM location. Black lines indicate constant dipole magnetic latitude and L shells.

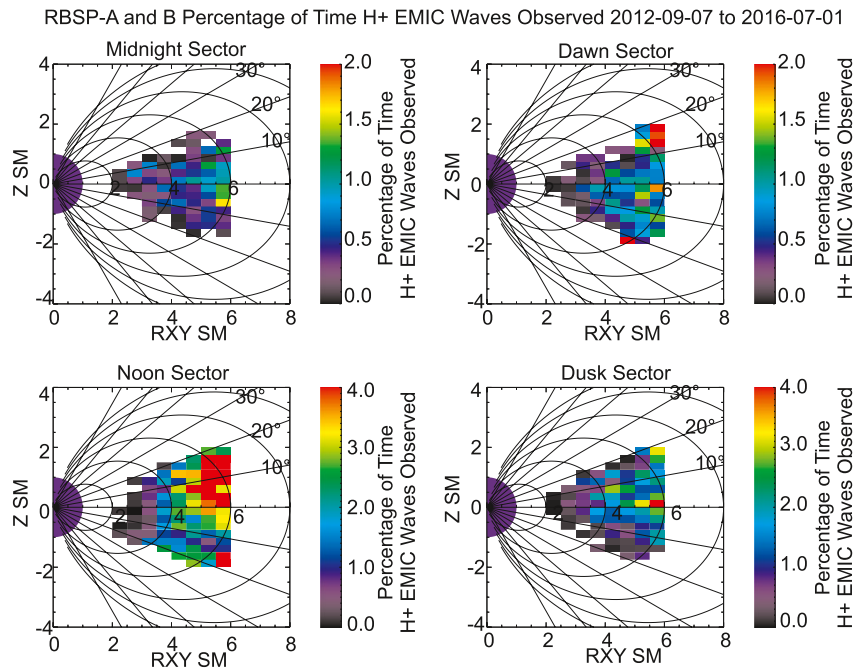


Figure 9. The occurrence rates of all H+ band EMIC waves as a function of R_{XY} and Z SM in the same format as Figure 8.

Figure 11 is in the same format as Figure 8, but for only the O+ band waves. Figure 11 reinforces the idea that the regions where O+ band EMIC waves are found is related to the plasma composition. In the midnight, dawn, and noon local time sectors, there are clusters of O+ band waves for $2 < R_{XY} < 4 R_E$ around the equatorial plane. In the noon and midnight sectors, there also appear to be a few observations of O+ band waves at higher latitudes and large radial distances. O+ band waves are spread out over the full range of latitudes and radial distances in the dusk sector. However, in the dusk sector, the greatest occurrence rates for O+ band waves are found near $+20^\circ$ latitude with a smaller peak near -20° .

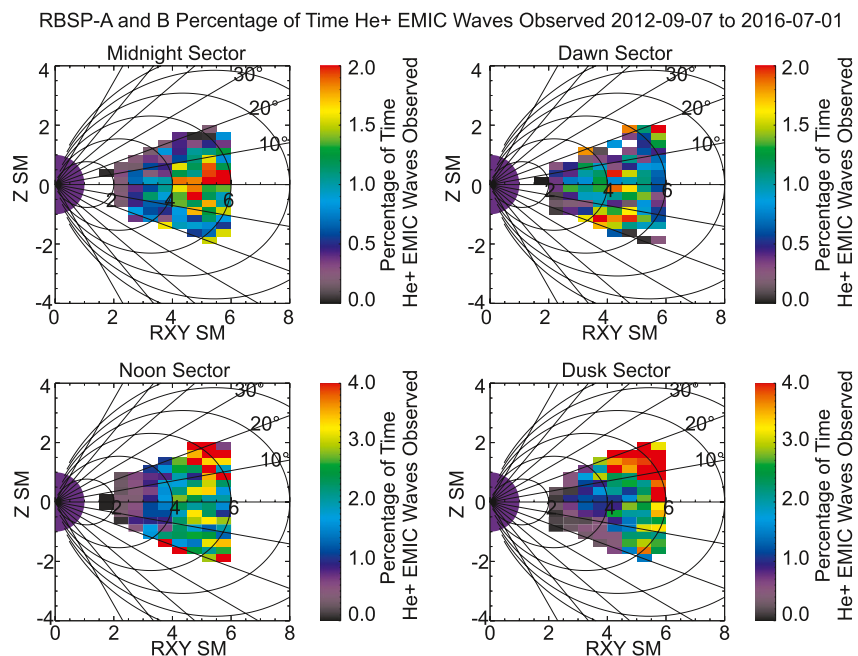


Figure 10. The occurrence rates of all He+ band EMIC waves as a function of R_{XY} and Z SM in the same format as Figure 8.

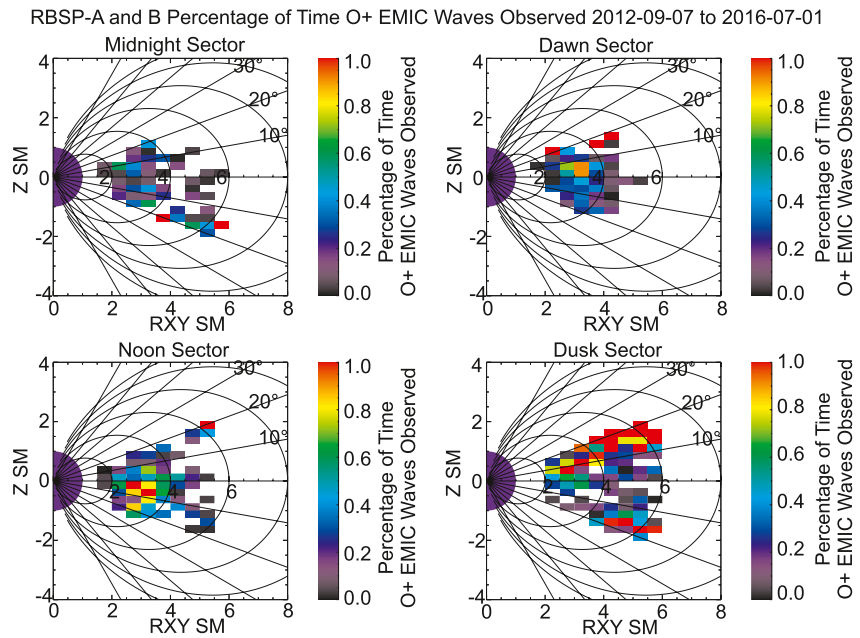


Figure 11. The occurrence rates of all O+ band EMIC waves as a function of R_{XY} and Z SM in the same format as Figure 8.

Figures 12 and 13 are in the same format as Figure 8, but for only H+ and He+ band waves with rising tones. Because we had so few EMIC wave observations with rising tones in the dawn sector, it is difficult to interpret the behavior of the waves in this region. In Figure 12 we can see that H+ band waves with rising tones in the midnight sector appeared to be clustered near the equatorial plane for $4 < R_{XY} < 6 R_E$. These events could have been associated with increases in ion anisotropy due to substorm injections. In the noon sector, H+ band waves with rising tones are spread out over $\pm 20^\circ$ latitude between $4 < R_{XY} < 6 R_E$. The distribution of He+ band waves with rising tones in the noon sector is not quite as concentrated, but has a similar pattern to the H+ band waves with rising tones. In the noon sector, the distributions of H+ and He+ band waves with rising tones suggest a possible connection to the effects of magnetospheric compressions. In the dusk sector, we have very

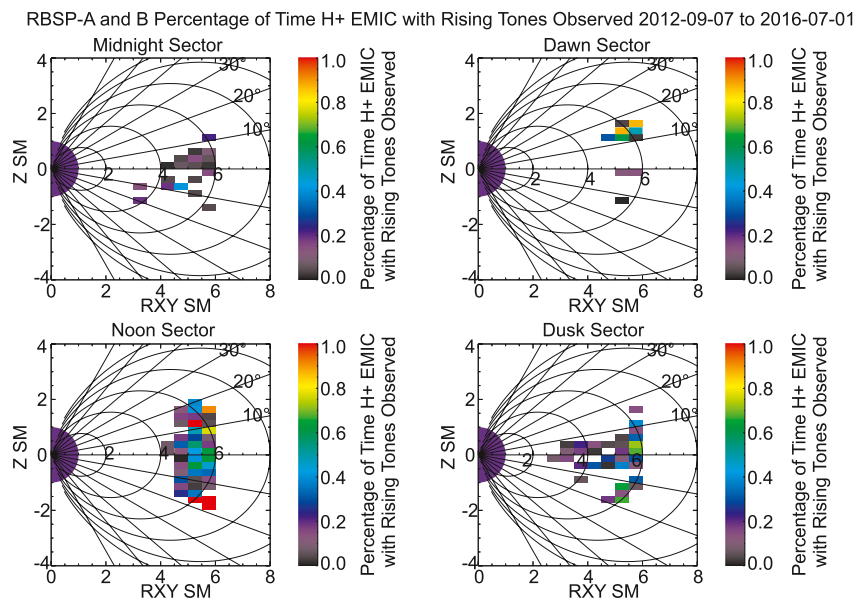


Figure 12. The occurrence rates of H+ band EMIC waves with rising tones as a function of R_{XY} and Z SM in the same format as Figure 8.

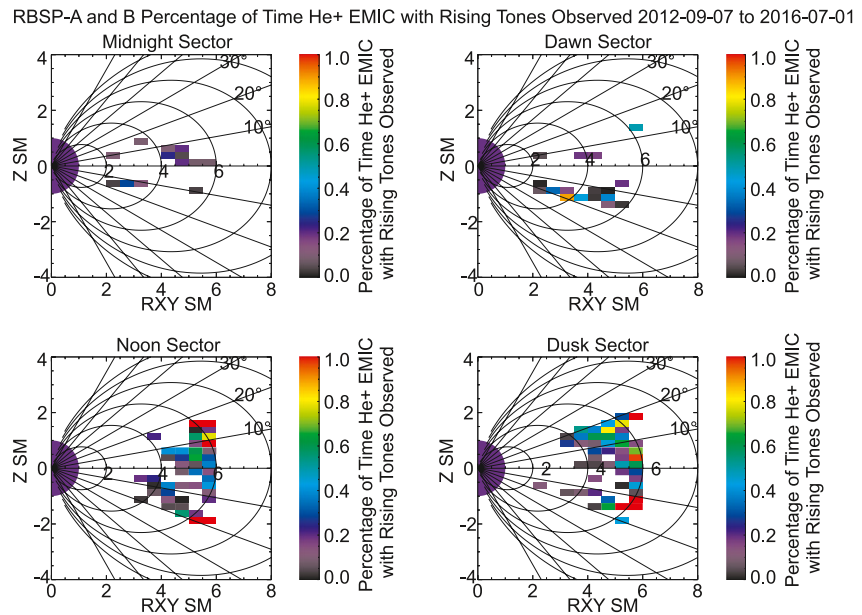


Figure 13. The occurrence rates of He+ band EMIC waves with rising tones as a function of R_{XY} and Z SM in the same format as Figure 8.

different distributions of H+ and He+ band waves with rising tones. Figure 12 shows that H+ band waves with rising tones in the dusk sector seem to mainly be found close to the equatorial plane, except near apogee. In contrast, Figure 13 shows the distribution of He+ band waves with rising tones in the dusk sector is spread out over radial distance and latitude, although there does appear to be a cluster of observations in the same region where the highest overall occurrence rates for He+ band waves in general are located. The differences between the locations where the H+ and He+ band waves with rising tones are found in the dusk sector could be related to plumes and other sources of plasma in this region.

6. Discussion

There have been many statistical studies of EMIC wave occurrence rates using satellite data. A table summarizing selected studies can be found in Wang et al. (2017). Some have examined overall EMIC wave occurrence rates as a function of L shell and MLT (e.g., Anderson et al., 1992a), or as a function of latitude (e.g., Allen et al., 2015). There have also been studies examining occurrence rates separately for the different EMIC wave bands (e.g., Saikin et al., 2015). However, many studies have focused on H+ and He+ band waves (e.g., Meredith et al., 2014; Min et al., 2012) and only a few have also included O+ band waves (e.g., Saikin et al., 2015). There have also been studies of polarizations and other wave properties (e.g., Anderson et al., 1992b; Min et al., 2012), and the effects of geomagnetic activity (e.g., Saikin et al., 2016; Usanova et al., 2012). A few studies have considered the occurrence of EMIC waves with rising tones (e.g., Grison et al., 2018; Nakamura et al., 2016). Comparing results from these studies can be difficult because of the ranges of L shells and magnetic latitudes covered, spatial bins used, and differences in EMIC wave selection conditions. These studies are also affected by the time spans included and where they fit into the solar cycle. In spite of the variations in methodologies and data coverage, results from past statistical studies and our work are complementary. The EMIC wave spatial scales in different MLT sectors (e.g., Blum et al., 2017), along with patterns in EMIC wave occurrence rates as a function of L shell, MLT, and magnetic latitude (MLAT), result from the sources of ion anisotropy, ion pitch angle distributions, and the effects of the plasma composition in different regions (e.g., Foster & Erickson, 2021; Lee et al., 2021; Usanova, 2021; Jun et al., 2021). In this section, we discuss some of these studies to place our results comparing the overall occurrence rates of EMIC waves and the occurrence rates of waves with rising tones into the broader context of EMIC waves throughout the magnetosphere.

6.1. Studies Examining Overall EMIC Wave Statistics as a Function of L and MLT

The Combined Release and Radiation Effects Satellite (CRRES) covered a comparable region of the inner magnetosphere to the Van Allen Probes but operated for only 15 months. Using CRRES data, Meredith et al. (2014) found He⁺ band EMIC waves with intensities greater than 0.1 nT^2 were most common during active conditions ($AE > 300 \text{ nT}$) between $4 < L^* < 7$ in the afternoon sector. They found H⁺ band EMIC waves with intensities greater than 0.1 nT^2 were most common in the afternoon sector in the same L^* range during active conditions, but with lower occurrence rates than the He⁺ band. Although it is difficult to directly compare occurrence rate percentages with Meredith et al. (2014), we agree with their result that H⁺ and He⁺ band waves are found most often in the afternoon sector.

Saikin et al. (2015) performed one of the first statistical studies of EMIC waves using the Van Allen Probes, and included observations from 8 September 2012 to 30 June 2014. Saikin et al. (2015) found two peaks in the H⁺ band occurrence rates, one from 9 to 12 MLT and another from 15 to 17 MLT. Saikin et al. (2016) did not consider EMIC waves by band, but they showed that waves are more likely to be observed by the Van Allen Probes in the pre-noon region during geomagnetically quiet periods. We did not find two distinct dayside peaks in H⁺ EMIC wave occurrence as in Saikin et al. (2015), but we do agree that there are broad regions of enhanced H⁺ and He⁺ band EMIC wave occurrence rates on the dayside from the pre-noon region to the afternoon region. Saikin et al. (2015) required a minimum 5-min dwell time for including EMIC wave events in their study, and we did not. However, this does not seem likely to be the reason for the difference between our H⁺ band results because the average lengths of the EMIC wave intervals we recorded were greater than 10 min. Since we found similar results for the overall percentage of events in each band, the differences between the locations of the H⁺ band occurrence rate peaks in our paper and those of Saikin et al. (2015) seem to be due to the different time periods included in our studies, as well as the larger MLT bin sizes we used.

Some studies of EMIC waves have included data from later in the Van Allen Probes mission than used by Saikin et al. (2015) and our study. Chen et al. (2019) studied EMIC wave occurrence rates in Van Allen Probes data from September 2012 through December 2017. Their overall occurrence distribution in L and MLT for the H⁺ band shows a broad region of EMIC wave activity across the dayside that agrees reasonably well with our results. For lower geomagnetic activity levels, Chen et al. (2019) found the peak in H⁺ band occurrence shifted toward the pre-noon region which supports the results of Saikin et al. (2016). However, Chen et al. (2019) found the He⁺ band peaks around $L \sim 3\text{--}4$ at all local times for all three ranges of geomagnetic activity they considered. Although we did see a weak, secondary peak in occurrence rates for He⁺ band waves around this L shell range, we found the greatest He⁺ occurrence rates in the afternoon sector at the largest L shells, in agreement with Saikin et al. (2015). Jun et al. (2021) studied occurrence rates of H⁺ and He⁺ band EMIC waves from 2017 to 2018 using Van Allen Probes and Arase data, which allowed them to cover a greater range of L shells. Jun et al. (2021) found H⁺ EMIC waves have two peak wave occurrence regions, one between 4 and 8 MLT for $L > 8$ and another at 10–14 MLT at $L < 6$ in the noon sector. They found high occurrence rates of He⁺ band waves from 12 to 21 MLT for $L = 6\text{--}8$, and between 14 and 18 MLT for $L > 8$. Although they only used two years of data, their results for the H⁺ and He⁺ EMIC waves are similar to Saikin et al. (2015) and our results for the $L < 6$ region covered by the Van Allen Probes. However, Jun et al. (2021) found that EMIC wave occurrence overall was greater for $L > 6$.

We found similar patterns of O⁺ band occurrence at low L shells to the Saikin et al. (2015) and Chen et al. (2019) studies using Van Allen Probes data. Van Allen Probes Helium, Oxygen, Proton, and Electron (HOPE) mass spectrometer data have shown that warm ($>30 \text{ eV}$) oxygen is most abundant closer to the plasmasphere boundary (Jahn et al., 2017). The region of peak EMIC wave occurrence rates for O⁺ band waves in Figure 6 is located in the vicinity of the peak in the quiet time median percent of total density for O⁺ during 2012–2015 in Jahn et al. (2017). This feature is related to the torus of warm oxygen plasma that wraps around the plasmasphere (e.g., Nosé et al., 2015). Yu et al. (2015) also found that in RBSP-A data from September 2012 to August 2014, O⁺ band EMIC waves seemed to be correlated with the region of the oxygen torus. Broadening in the region of O⁺ band EMIC wave occurrence on the dayside in Figure 6 could be associated with the warm plasma cloak (e.g., Chappell et al., 2008) that drapes over the nightside plasmasphere and is carried into the morning and early afternoon sectors by the sunward convective wind in the magnetosphere. In Figure 11, the high latitude observations of O⁺ EMIC band waves in the dusk sector suggest that EMIC waves can also have connections to ion outflows and plasmaspheric drainage plumes. Foster and Erickson (2021) presented a case study using Van Allen

Probes data when outflows of ionospheric oxygen were observed near dusk in the vicinity of a plasmaspheric plume along with He+ band EMIC waves. Although the waves during this event were in the He+ band, Foster and Erickson (2021) demonstrated that outflows of O+ ions can be associated with EMIC waves observed by the Van Allen Probes.

Studies of EMIC waves using spacecraft that provided coverage at higher L shells, have mainly considered overall EMIC wave statistics or the H+ and He+ bands. Anderson et al. (1992a, 1992b) used Active Magnetospheric Particle Tracer Explorers (AMPTE) Charge Composition Explorer (CCE) data from one complete local time precession (1984–1985) to construct occurrence distributions of EMIC waves from $L \sim 3.5$ to 9, and found the highest concentration of EMIC waves in the afternoon region. Keika et al. (2013) examined EMIC wave occurrence rates for the entire AMPTE/CCE mission from August 1984 to January 1989. They found peak occurrence of H+ band waves for $L \geq 7$ in the afternoon sector, but during quiet conditions, H+ band waves may be found on the morning side. Keika et al. (2013) also found He+ band waves mainly occur for $L \geq 7$ in the afternoon sector under quiet conditions, and in the inner magnetosphere for $L < 7$ on the prenoon to duskside region under disturbed conditions. They proposed H+ band waves were generated by solar wind compressions, which lead to perpendicular adiabatic ion heating and an increase in temperature anisotropy, and the He+ band waves were related to injections of plasma sheet ions.

Using THEMIS data from May 2007 to December 2011, Usanova et al. (2012) found the highest EMIC occurrence rates in the noon and dusk sectors, consistent with the westward direction of the energetic ion drifts. They also found EMIC wave occurrence rates increase toward the magnetopause, with quiet time EMIC activity typically being a dayside outer magnetosphere phenomenon. Although Usanova et al. (2012) generally found low occurrence rates inside geosynchronous orbit compared to higher L shells, there was increased EMIC wave activity in the inner magnetosphere in the dusk sector for higher solar wind dynamic pressures. Min et al. (2012) also studied EMIC wave occurrence rates and polarizations using THEMIS data from April 2007 to December 2010. Most of their EMIC wave events were at distances greater than $6 R_E$. Min et al. (2012) found He+ band waves had peak occurrence rates near dusk from 8 to $12 R_E$. H+ band occurrence rates had a maximum in the morning sector from 10 to $12 R_E$ with a secondary peak from noon to dusk. The peak near dawn was not seen in Anderson et al. (1992a) because that investigation was limited to $9.5 R_E$. Case studies using THEMIS have shown that EMIC waves can be observed all the way out to the magnetopause in the afternoon sector (Sigsbee et al., 2016) where they may be associated with enhanced densities in plasmaspheric drainage plumes (e.g., Morley et al., 2009; Fraser et al., 2010; Halford et al., 2015; Yuan et al., 2012, 2013). Grison et al. (2021) found THEMIS EMIC wave occurrence rates have a maximum within two R_E of the magnetopause, or about 7–10 R_E away from Earth in the noon sector. They also found the regions of peak EMIC wave occurrence were closer to Earth near dusk than at dawn, which they attributed to local time asymmetries in magnetosheath conditions and the sources of energetic ions on the nightside. Using Magnetospheric Multiscale (MMS) data, Wang et al. (2017) found H+ band EMIC waves mostly occur for $L > 5$ while He+ band EMIC waves are more frequently observed for $L < 6$. They also found the occurrence rate of H+ band waves is higher on the dayside than the nightside, with peak occurrence rates in the post-noon sector for $5 < L < 8$, and a smaller, secondary peak in the dawn sector.

The studies using AMPTE/CCE, THEMIS, MMS, Arase, and the Van Allen Probes, we discussed show the peak regions for EMIC wave occurrence depend on the wave band, geomagnetic activity levels, and L shell. We found the peak regions for EMIC wave occurrence in the H+ and He+ band are mainly from noon to dusk, close to the Van Allen Probes' apogee, while O+ band waves are often found closer to Earth at a wider range of MLT. Other studies indicate there can also be a secondary peak for H+ band waves near dawn, which appears to mainly result from waves observed during quiet times and is usually found for larger L shells than those covered by the Van Allen Probes. The studies we discussed also tell us the regions where EMIC waves can occur have a large extent in radial distance or L shell. Tetrick et al. (2017) found most EMIC waves observed by the Van Allen Probes occurred within -1 to $+2 R_E$ relative to the plasmopause, while studies using AMPTE/CCE, THEMIS, and MMS have shown high occurrence rates further away from Earth. Although there is a statistically large range of L shells where EMIC waves may be found, studies have suggested that individual EMIC wave events may be narrow in L shell but more extended in MLT and UT. (e.g., Blum et al., 2017, 2016). The Van Allen Probes may not have fully covered the L shell range of the greatest EMIC wave occurrence rates, but their orbits provided coverage of the regions where EMIC waves are most likely to affect radiation belt dynamics.

6.2. Studies Examining Overall EMIC Wave Statistics as a Function of Latitude

The Jun et al. (2021) study of Van Allen Probes and Arase data mentioned previously also examined the overall EMIC wave occurrence rates as a function of magnetic latitude (MLAT). They found occurrence rate peaks in the morning sector from 4 to 8 MLT for $MLAT < -30^\circ$ with $L > 8$, in the noon sector from 10 to 14 MLT for $|MLAT| < 20^\circ$ with $L = 3-6$, and in the afternoon/dusk sector from 12 to 21 MLT for $MLAT > 20^\circ$ with $L = 6-12$. Jun et al. (2021) examined the $|MLAT|$ dependence of H+ and He+ band EMIC wave polarizations, but did not consider occurrence rates as a function of $|MLAT|$ for each frequency band, as we did. We only covered $\pm 20^\circ$ MLAT using just Van Allen Probes data, but our Figure 8 also has peaks off the equatorial plane in the dusk sector. Our Figures 10 and 11 show that the off-equatorial peaks near dusk are mainly due to He+ and O+ band waves. The Chen et al. (2019) study of Van Allen Probes data mentioned in the previous section examined occurrence rates separately for the H+, He+, and O+ EMIC wave bands in the L -MLAT plane, but did not consider each MLT sector, as we did. They found EMIC waves were mainly observed for $|MLAT| < 10^\circ$, and that the peak regions for the O+ band and He+ were closer to Earth than for the H+ band. We obtained very different results from Chen et al. (2019). As shown by our Figures 8–11, we found off-equatorial peaks in occurrence rates in the noon and dusk sectors, and that the He+ band can be observed over a wide range of radial distance. Our Figure 11 shows O+ band waves in the dawn and noon sectors were observed closer to Earth, but in the dusk sector they covered a wide range of radial distances. As discussed previously, the higher latitude observations of O+ EMIC band waves near dusk in Figure 11 suggest possible connections to ion outflows and plasmaspheric drainage plumes.

Allen et al. (2015, 2016) used data from the polar orbiting Cluster mission from 2001 to 2010 to examine the dependence of EMIC wave occurrence and properties on MLAT, L shell, and MLT. They did not split up the observations by EMIC wave band. Allen et al. (2015, 2016) attributed peaks in EMIC wave occurrence as a function of L and MLAT in different local time sectors to three sources. Peaks in EMIC wave occurrence in the post-noon to dusk sector at middle L -shells ($\sim 8-11$) and low $|MLAT|$ ($< 15^\circ$) found by Allen et al. (2015) were associated with overlap between cold plasmaspheric or plume populations with hot anisotropic ring current populations by Allen et al. (2016). Peaks in EMIC wave occurrence identified by Allen et al. (2015) all along the dayside magnetosphere at high L shells and low $|MLAT|$ were likely related to dayside magnetospheric compression and drift shell splitting (Allen et al., 2016). The Van Allen Probes covered lower L shells than Cluster, but the locations of the peaks in EMIC wave occurrence in Figures 8–13 are mostly consistent with the conclusions of Allen et al. (2015, 2016) regarding the plasma populations responsible for EMIC waves in different local time sectors at the lower MLAT values. Allen et al. (2015, 2016) proposed peaks in EMIC wave occurrence in off-equator regions ($MLAT \sim 25^\circ$ in dawn/dusk and $\sim 30^\circ$ in noon) and high L -shells (~ 10 in dawn/dusk and ~ 8 in noon) were likely due to wave generation from particles executing Shabansky orbits (e.g., McCollough et al., 2010, 2012). Due to the range of L shells and MLAT covered by the Van Allen Probes, it seems unlikely that the peaks in the overall EMIC wave statistics shown in Figure 8 as a function of R_{XY} and Z SM are mainly due to Shabansky orbits. However, case studies have shown EMIC waves observed by the Van Allen Probes on the dayside can be related to magnetospheric compressions (e.g. Sigsbee et al., 2020; Engebretson et al., 2015). The EMIC wave events contributing to the overall occurrence rate peaks in Figure 8 off the equatorial plane in the noon and dusk sectors may be associated with magnetospheric compressions, while events near the equatorial plane could result from overlap between plume populations and the ring current.

6.3. Studies Examining Statistics of EMIC Waves With Rising Tones

There have not been many studies of occurrence rates for EMIC waves with rising tones because they were only recognized as a distinct subset of EMIC waves about 11 years ago (Omura et al., 2010; Pickett et al., 2010). One of the first surveys of EMIC waves with rising tones was made by visually inspecting spectrograms of Cluster STAFF-SC data along the spacecraft spin axis from 2000 to 2008 (Grison et al., 2013). This study found unambiguous cases on only three different days, all of which were observed at the plasmopause between 22 and 24 magnetic local time (MLT) and between $\pm 15^\circ$ magnetic latitude. Grison et al. (2013) also presented the first observations of triggered emissions below the local He+ gyrofrequency. When Grison et al. (2018) revisited the Cluster data set, they attributed the lack of rising tones in their 2013 paper to the scales used on the spectrograms and weak power spectral density along the spin axis. Grison et al. (2018) examined Cluster data during 935 individual crossings of plasmaspheric plumes from February 2001 to February 2006, which corresponded

to 189 unique plume events. Because of Cluster's polar orbit, all of the plume crossings were off the magnetic equatorial plane. Grison et al. (2018) compared the occurrence rates of broadband, narrowband, and rising tone emissions below the proton gyrofrequency (1–10 Hz) during these plume events. Broadband emissions were most common and observed in 67% of the 189 plumes, followed by narrowband emissions (in 16% of the plumes) and EMIC rising tones (only 3% of the plumes). The rising tones were found between $17^\circ \leq |\text{MLAT}| \leq 35^\circ$ and most occurred on the dayside between 11 and 16 MLT. Results of ray tracing analysis performed by Grison et al. (2018) suggested these rising tones were triggered locally and related to the EMIC source region found above 15° MLAT by Allen et al. (2016) where particles may be executing Shabansky orbits (McCollough et al., 2012).

Although we did not specifically screen for plumes in our study, we found cases of EMIC waves with rising tones in the region where plumes are observed. The occurrence distributions of H+ EMIC waves with rising tones as a function of R_{XY} and Z SM shown in Figure 12 for the noon sector and dusk sector appear consistent with the conclusions of past studies (Allen et al., 2015, 2016; Grison et al., 2018; Jun et al., 2021) regarding the latitude distributions and primary sources of free energy to drive EMIC waves in different local time sectors. However, the occurrence distributions of He+ band waves with rising tones as a function of R_{XY} and Z SM shown in Figure 13 do not clearly show the latitude distributions expected if the waves are associated with compressions near noon and interactions between plumes and the ring current near dusk.

Nakamura et al. (2014) used THEMIS high-resolution fluxgate magnetometer (FGM) data (FGH) from May 2007 and December 2011 to search for EMIC rising tone emissions in the inner magnetosphere. They found very few cases near the plasmopause between 3 and $6 R_E$, but found a few tens of events with high-resolution data at distances greater than $7 R_E$. They found EMIC waves with rising tones in both the H+ and He+ bands, and strong rising tone emissions associated with magnetospheric compressions due to the solar wind. Nakamura et al. (2014) also found that the magnetic footprint of one THEMIS probe was located near a ground magnetometer station that observed Pc1 waves with similar rising tone spectra during one event. Nakamura et al. (2014) attributed the small number of cases identified to the extremely low availability of the FGH data, which were recorded for only a few tens of minutes per day.

Nakamura et al. (2016) conducted a second survey of the THEMIS data from January 2012 to December 2014 for radial distances greater than $5 R_E$ using the low resolution FGM data (FGL). The FGL data had better availability, but couldn't detect EMIC waves closer to Earth because the H+ cyclotron frequency exceeds 2 Hz. Nakamura et al. (2016) automatically classified spectra as rising tones, falling tones, ambiguous tones, and non-emission events using an algorithm based upon rising tone characteristics from their 2014 study. To identify EMIC wave events, they divided the data into 20-min segments, applied filters to select the H+ frequency band, and used Morlet wavelets to obtain dynamic spectra and wave polarizations. Then they classified each 20-min data segment based upon on frequency sweep rates df/dt and amplitude variations ΔB in the dynamic spectra. They did not place time constraints on features identified by the algorithm, and their database includes both groups of rising and falling tones repeating with short periods (less than 10 s), as well as longer duration structures. Nakamura et al. (2016) found that more than 30% of the total EMIC wave events in the THEMIS data set had EMIC rising or falling tones, and that the occurrence rate of rising tone events is slightly greater than that of falling tone events. The EMIC waves with rising or falling tones were most likely to be found in a broad region across the dayside, where many studies have found EMIC waves are likely to occur. Our Figures 6, 12, and 13 show that we found EMIC waves with rising tones mainly occur on the dayside, which agrees with the results of Nakamura et al. (2016) on the preferred MLT regions for these waves.

Because the necessary high-resolution THEMIS data were not available for $L < 5$, Nakamura et al. (2016) could not compare occurrence rates of all EMIC waves to those with rising tones in the regions of the inner magnetosphere that are of key importance to radiation belt dynamics and particle scattering, as we were able to do using the Van Allen Probes. Using Van Allen Probes data, we found most of the H+ rising tones between L shells of 4–6, with a few cases for $L < 4$. This region was not covered fully by either the Cluster and THEMIS surveys of EMIC waves with rising tones. Nakamura et al. (2016) found a much greater percentage of the total EMIC wave events in the THEMIS data set had EMIC rising or falling tones than we found in the Van Allen Probes data set, as shown by Tables 1–3. Comparison to past studies of EMIC waves using satellites that covered larger radial distances than the Van Allen Probes suggests that we may not have been able to fully sample the regions of greatest occurrence for EMIC waves in general, and thus we observed fewer rising tones than the studies using THEMIS data. However, the methodologies used to select events also likely contributed to the differences

between our results for the percentages of EMIC wave events with rising tones. The Nakamura et al. (2016) study using data from THEMIS compared occurrence distributions for all EMIC waves to those with rising tones as a function of L and MLT, but did not consider the individual frequency bands or look at occurrence rates as a function of latitude or distance from the equatorial plane, as we did. In Figures 12 and 13, the peak regions for the occurrence of waves with rising tones as a function of R_{XY} and Z SM indicate the rising tones may have been associated with magnetospheric compressions, which usually result in disturbed geomagnetic conditions. Nakamura et al. (2016) found EMIC waves with rising or falling tones tend to be generated under disturbed magnetospheric conditions, which supports this conclusion.

7. Conclusions

We performed a statistical analysis of the overall occurrence rates of EMIC waves, as well as the occurrence rates of EMIC waves in the H+, He+, and O+ frequency bands, and the occurrence rates of EMIC waves with rising tones in the H+ and He+ bands using Van Allen Probes data from 2012 to 2016.

1. For all EMIC waves, peak EMIC wave occurrence rates were found between noon and 18 MLT, with the peak covering the broadest range of L shells around 15 MLT. As a function of R_{XY} and Z SM, we found peak occurrence rates in the noon sector between $4 < R_{XY} < 6 R_E$ and $-1 < Z < 2 R_E$ (-10° – 20° MLAT) and in the dusk sector between $5 < R_{XY} < 6 R_E$ and $0 < Z < 2 R_E$ (0° – 20° MLAT).
2. For all EMIC waves in the H+ band, peak occurrence rates as a function of L and MLT were found between 11 and 16 MLT. As a function of R_{XY} and Z SM, we found peak occurrence rates in the noon sector between $4 < R_{XY} < 6 R_E$ and $0 < Z < 2 R_E$ (0° – 20° MLAT).
3. For all He+ band EMIC waves, peak occurrence rates as a function of L and MLT were found from $4 < L < 6$ between noon and 18 MLT. As a function of R_{XY} and Z SM, peak occurrence rates were found in the midnight sector close to the equatorial plane, and in the noon and dusk sectors between $4 < R_{XY} < 6 R_E$ and $1 < Z < 2 R_E$ (10° – 20° MLAT).
4. For O+ band EMIC waves, peak occurrence rates were found between $2 < L < 4$ over a broad range of MLT, and at higher L values near dusk. As a function of R_{XY} and Z SM, O+ band waves were clustered between $2 < R_{XY} < 4 R_E$ within $Z \sim \pm 1 R_E$ in the midnight, dawn, and noon sectors, consistent with the location of the oxygen torus. In the dusk sector, peak occurrence rates for O+ band waves were found from $2 < R_{XY} < 6 R_E$ at about $\sim 20^\circ$ MLAT.
5. About 7%–8% of H+ and He+ band EMIC waves have rising tones. H+ band rising tones generally appear to be triggered emission type events that rise out of the main band of EMIC waves, while He+ band rising tones are often embedded within the main band of EMIC waves.
6. H+ and He+ band waves with rising tones were found mainly at larger L shells, from 8 to 18 MLT, with very few events from midnight to dawn. As a function of R and Z SM, H+ band waves with rising tones were found between $4 < R_{XY} < 6 R_E$ and $Z \sim \pm 2 R_E$ ($\pm 20^\circ$ MLAT) in the noon sector, while events in the dusk sector were mostly found near the equatorial plane. He+ band waves with rising tones were distributed throughout the noon and dusk sectors between $4 < R_{XY} < 6 R_E$ and $Z \sim \pm 2 R_E$ ($\pm 20^\circ$ MLAT).

Data Availability Statement

The Autoplot interactive data browser is available from <http://autoplot.org/>. Data from the Van Allen Probes can be obtained through the Van Allen Probes Science Gateway (<http://rbpsgway.jhuapl.edu/>) and NASA CDAWeb (<https://cdaweb.gsfc.nasa.gov/>). Kletzing (2022a, 2022b).

References

- Allen, R. C., Zhang, J.-C., Kistler, L. M., Spence, H. E., Lin, R.-L., Klecker, B., et al. (2015). A statistical study of EMIC waves observed by cluster: 1. Wave properties. *Journal of Geophysical Research: Space Physics*, *120*(7), 5574–5592. <https://doi.org/10.1002/2015JA021333>
- Allen, R. C., Zhang, J.-C., Kistler, L. M., Spence, H. E., Lin, R.-L., Klecker, B., et al. (2016). A statistical study of EMIC waves observed by cluster: 2. Associated plasma conditions. *Journal of Geophysical Research: Space Physics*, *121*(7), 6458–6479. <https://doi.org/10.1002/2016JA022541>
- Anderson, B., Erlandson, R., & Zanetti, L. (1992a). A statistical study of Pc 1-2 magnetic pulsations in the equatorial magnetosphere, 1. Equatorial occurrence distributions. *Journal of Geophysical Research*, *97*(A3), 3075–3088. <https://doi.org/10.1029/91ja02706>
- Anderson, B., Erlandson, R., & Zanetti, L. (1992b). A statistical study of Pc 1-2 magnetic pulsations in the equatorial magnetosphere, 2. Wave properties. *Journal of Geophysical Research*, *97*(A3), 3089–3101. <https://doi.org/10.1029/91ja02697>

Acknowledgments

This work was supported by National Aeronautics and Space Administration: JHU/APL Contract No. 921647 under Prime Contract No. NAS5-01072 and 80NSSC20K0690.

- Bashir, M. F., & Ilie, R. (2018). A new N+ band of electromagnetic ion cyclotron waves in multi-ion cold plasmas. *Geophysical Research Letters*, 45(19), 10150–10159. <https://doi.org/10.1029/2018GL080280>
- Bashir, M. F., & Ilie, R. (2021). The first observation of N+ electromagnetic ion cyclotron waves. *Journal of Geophysical Research: Space Physics*, 126(3), e2020JA028716. <https://doi.org/10.1029/2020JA028716>
- Bevington, P. R., & Robinson, D. K. (2003). *Data reduction and error analysis for the physical sciences* (3rd ed.). McGraw-Hill Higher Education.
- Bingley, L., Angelopoulos, V., Sibeck, D., Zhang, X., & Halford, A. (2019). The evolution of a pitch-angle “bite-out” scattering signature caused by EMIC wave activity: A case study. *Journal of Geophysical Research: Space Physics*, 124(7), 5042–5055. <https://doi.org/10.1029/2018JA026292>
- Blum, L. W., Agapitov, O., Bonnell, J. W., Kletzing, C., & Wygant, J. (2016). EMIC wave spatial and coherence scales as determined from multi-point Van Allen Probe measurements. *Geophysical Research Letters*, 43(10), 4799–4807. <https://doi.org/10.1002/2016GL068799>
- Blum, L. W., Bonnell, J. W., Agapitov, O., Paulson, K., & Kletzing, C. (2017). EMIC wave scale size in the inner magnetosphere: Observations from the dual Van Allen Probes. *Geophysical Research Letters*, 44(3), 1227–1233. <https://doi.org/10.1002/2016GL072316>
- Bortnik, J., Thorne, R. M., O'Brien, T. P., Green, J. C., Strangeway, R. J., Shprits, Y. Y., & Baker, D. N. (2006). Observation of two distinct, rapid loss mechanisms during the 20 November 2003 radiation belt dropout event. *Journal of Geophysical Research*, 111(A12), A12216. <https://doi.org/10.1029/2006JA011802>
- Chappell, C. R., Huddleston, M. M., Moore, T. E., Giles, B. L., & Delcourt, D. C. (2008). Observations of the warm plasma cloak and an explanation of its formation in the magnetosphere. *Journal of Geophysical Research*, 113(A9), A09206. <https://doi.org/10.1029/2007JA012945>
- Chen, H., Gao, X., Lu, Q., & Wang, S. (2019). Analyzing EMIC waves in the inner magnetosphere using long-term Van Allen Probes observations. *Journal of Geophysical Research: Space Physics*, 124(9), 7402–7412. <https://doi.org/10.1029/2019JA026965>
- Cornwall, J. M. (1965). Cyclotron instabilities and electromagnetic emission in the ultra low frequency and very low frequency ranges. *Journal of Geophysical Research*, 70(1), 61–69. <https://doi.org/10.1029/JZ070i001p00061>
- Cornwall, J. M., & Schulz, M. (1971). Electromagnetic ion-cyclotron instabilities in multicomponent magnetospheric plasmas. *Journal of Geophysical Research*, 76(31), 7791–7796. <https://doi.org/10.1029/JA076i031p07791>
- Denton, R. E., Jordanova, V. K., & Fraser, B. J. (2014). Effect of spatial density variation and O+ concentration on the growth and evolution of electromagnetic ion cyclotron waves. *Journal of Geophysical Research: Space Physics*, 119(10), 8372–8395. <https://doi.org/10.1002/2014JA020384>
- Engebretson, M. J., Posch, J. L., Wygant, J. R., Kletzing, C. A., Lessard, M. R., Huang, C.-L., et al. (2015). Van Allen Probes, NOAA, GOES, and ground observations of an intense EMIC wave event extending over 12 h in magnetic local time. *Journal of Geophysical Research: Space Physics*, 120(7), 5465–5488. <https://doi.org/10.1002/2015JA021227>
- Erlanson, R. E., Anderson, B. J., & Zanetti, L. J. (1992). Viking magnetic and electric field observations of periodic Pc1 waves: Pearl pulsations. *Journal of Geophysical Research*, 97(A10), 14823–14832. <https://doi.org/10.1029/92JA00838>
- Faden, J. B., Weigel, R. S., Merka, J., & Friedel, R. H. W. (2010). Autoplot: A browser for scientific data on the web. *Earth Science Informatics*, 3(Issue 1–2), 41–49. <https://doi.org/10.1007/s12145-010-0049-0>
- Fok, M.-C., Khazanov, G. V., Krivovrutsky, E. N., & Gloer, A. (2016). Convective growth of electromagnetic ion cyclotron waves from realistic ring current ion distributions. *Journal of Geophysical Research: Space Physics*, 121(11), 10966–10977. <https://doi.org/10.1002/2016JA022964>
- Foster, J. C., & Erickson, P. J. (2021). Van Allen probes observations of oxygen ions at the geospace plume. *Frontiers in Astronomy and Space Sciences*, 8, 705637. <https://doi.org/10.3389/fspas.2021.705637>
- Fraser, B. J., Grew, R. S., Morley, S. K., Green, J. C., Singer, H. J., Loto'aniu, T. M., & Thomsen, M. F. (2010). Storm time observations of electromagnetic ion cyclotron waves at geosynchronous orbit: GOES results. *Journal of Geophysical Research*, 115(A5), A05208. <https://doi.org/10.1029/2009JA014516>
- Gomberoff, L., & Neira, R. (1983). Convective growth rate of ion cyclotron waves in a H+–He+ and H+–He+–O+ plasma. *Journal of Geophysical Research*, 88(A3), 2170–2174. <https://doi.org/10.1029/JA088iA03p02170>
- Green, J. C., Onsager, T. G., O'Brien, T. P., & Baker, D. N. (2004). Testing loss mechanisms capable of rapidly depleting relativistic electron flux in the Earth's outer radiation belt. *Journal of Geophysical Research*, 109(A12), A12211. <https://doi.org/10.1029/2004JA010579>
- Grison, B., Darrouzet, F., Santolík, O., Cornilleau-Wehrlin, N., & Masson, A. (2016). Cluster observations of reflected EMIC-triggered emission. *Geophysical Research Letters*, 43(9), 4164–4171. <https://doi.org/10.1002/2016GL069096>
- Grison, B., Hanzelka, M., Breuillard, H., Darrouzet, F., Santolík, O., Cornilleau-Wehrlin, N., & Dandouras, I. (2018). Plasmaspheric plumes and EMIC rising tone emissions. *Journal of Geophysical Research: Space Physics*, 123(11), 9443–9452. <https://doi.org/10.1029/2018JA025796>
- Grison, B., Santolík, O., Cornilleau-Wehrlin, N., Masson, A., Engebretson, M. J., Pickett, J. S., et al. (2013). EMIC triggered chorus emissions in Cluster data. *Journal of Geophysical Research: Space Physics*, 118(3), 1159–1169. <https://doi.org/10.1002/jgra.50178>
- Grison, B., Santolík, O., Lukačević, J., & Usanova, M. E. (2021). Occurrence of EMIC waves in the magnetosphere according to their distance to the magnetopause. *Geophysical Research Letters*, 48(3), e2020GL090921. <https://doi.org/10.1029/2020GL090921>
- Halford, A., Fraser, B. J., & Morley, S. K. (2015). EMIC waves and plasmaspheric plume density: CRRES results. *Journal of Geophysical Research*, 120(3), 1974–1992. <https://doi.org/10.1002/2014JA020338>
- He, Z., Zong, Q., Liu, S., Wang, Y., Lin, R., & Shi, L. (2014). Frequency sweep rates of rising tone electromagnetic ion cyclotron waves: Comparison between nonlinear theory and Cluster observation. *Physics of Plasmas*, 21(12), 122309. <https://doi.org/10.1063/1.4905065>
- Hendry, A. T., Rodger, C. J., & Clilverd, M. A. (2017). Evidence of sub-MeV EMIC-driven electron precipitation. *Geophysical Research Letters*, 44(3), 1210–1218. <https://doi.org/10.1002/2016GL071807>
- Hendry, A. T., Rodger, C. J., Clilverd, M. A., Engebretson, M. J., Mann, I. R., Lessard, M. R., et al. (2016). Confirmation of EMIC wave-driven relativistic electron precipitation. *Journal of Geophysical Research: Space Physics*, 121(6), 5366–5383. <https://doi.org/10.1002/2015JA022224>
- Horne, R., & Thorne, R. (1994). Convective instabilities of electromagnetic ion cyclotron waves in the outer magnetosphere. *Journal of Geophysical Research*, 99(A9), 17259–17273. <https://doi.org/10.1029/94JA01259>
- Jacobs, J. A., Kato, Y., Matsushita, S., & Troitskaya, V. A. (1964). Classification of geomagnetic micropulsations. *Journal of Geophysical Research*, 69(1), 180–181. <https://doi.org/10.1029/jz069i001p00180>
- Jahn, J.-M., Goldstein, J., Reeves, G. D., Fernandes, P. A., Skoug, R. M., Larsen, B. A., & Spence, H. E. (2017). The warm plasma composition in the inner magnetosphere during 2012–2015. *Journal of Geophysical Research: Space Physics*, 122(11), 11018–11043. <https://doi.org/10.1002/2017JA024183>
- Jordanova, V. K., Farrugia, C. J., Thorne, R. M., Khazanov, G. V., Reeves, G. D., & Thomsen, M. F. (2001). Modeling ring current proton precipitation by electromagnetic ion cyclotron waves during the May 14–16, 1997, storm. *Journal of Geophysical Research*, 106(A1), 7–22. <https://doi.org/10.1029/2000JA002008>

- Jun, C.-W., Miyoshi, Y., Kurita, S., Yue, C., Bortnik, J., Lyons, L., et al. (2021). The characteristics of EMIC waves in the magnetosphere based on the Van Allen Probes and Arase observations. *Journal of Geophysical Research: Space Physics*, 126(6), e2020JA029001. <https://doi.org/10.1029/2020JA029001>
- Keika, K., Takahashi, K., Ukhorskiy, A. Y., & Miyoshi, Y. (2013). Global characteristics of electromagnetic ion cyclotron waves: Occurrence rate and its storm dependence. *Journal of Geophysical Research: Space Physics*, 118(7), 4135–4150. <https://doi.org/10.1002/jgra.50385>
- Kim, E.-H., Johnson, J. R., Kim, H., & Lee, D.-H. (2015). Inferring magnetospheric heavy ion density using EMIC waves. *Journal of Geophysical Research: Space Physics*, 120(8), 6464–6473. <https://doi.org/10.1002/2015JA021092>
- Kim, H., Lessard, M. R., Engebretson, M. J., & Young, M. A. (2011). Statistical study of Pc1–2 wave propagation characteristics in the high-latitude ionospheric waveguide. *Journal of Geophysical Research*, 116(A7), A07227. <https://doi.org/10.1029/2010JA016355>
- Kim, H.-J., & Chan, A. A. (1997). Fully adiabatic changes in storm time relativistic electron fluxes. *Journal of Geophysical Research*, 102(A10), 22107–22116. <https://doi.org/10.1029/97JA01814>
- Kletzing, C. A. (2022a). Van Allen Probe A fluxgate magnetometer high resolution data in SM coordinates [Dataset]. NASA Space Physics Data Facility. <https://doi.org/10.48322/h47r-sf90>
- Kletzing, C. A. (2022b). Van Allen Probe B fluxgate magnetometer high resolution data in SM coordinates [Dataset]. NASA Space Physics Data Facility. <https://doi.org/10.48322/k10e-1w74>
- Kletzing, C. A., Kurth, W. S., Acuna, M., MacDowall, R. J., Torbert, R. B., Averkamp, T., et al. (2013). The electric and magnetic field instrument suite and integrated science (EMFISIS) on RBSP. *Space Science Reviews*, 179(1–4), 127–181. <https://doi.org/10.1007/s11214-013-9993-6>
- Kozyra, J., Cravens, T., Nagy, A., Fonthelm, E., & Ong, R. (1984). Effects of energetic heavy ions on electromagnetic ion cyclotron wave generation in the plasmopause region. *Journal of Geophysical Research*, 89(A4), 2217–2233. <https://doi.org/10.1029/ja089ia04p02217>
- Kubota, Y., & Omura, Y. (2017). Rapid precipitation of radiation belt electrons induced by EMIC rising tone emissions localized in longitude inside and outside the plasmopause. *Journal of Geophysical Research: Space Physics*, 122(1), 293–309. <https://doi.org/10.1002/2016JA023267>
- Kubota, Y., Omura, Y., & Summers, D. (2015). Relativistic electron precipitation induced by EMIC-triggered emissions in a dipole magnetosphere. *Journal of Geophysical Research: Space Physics*, 120(6), 4384–4399. <https://doi.org/10.1002/2015JA021017>
- Lee, D.-Y., Noh, S.-J., Choi, C.-R., Lee, J. J., & Hwang, J. A. (2017). Effect of hot anisotropic He⁺ ions on the growth and damping of electromagnetic ion cyclotron waves in the inner magnetosphere. *Journal of Geophysical Research: Space Physics*, 122(5), 4935–4942. <https://doi.org/10.1002/2016JA023826>
- Lee, J. H., Blum, L. W., & Chen, L. (2021). On the impacts of ions of ionospheric origin and their composition on Magnetospheric EMIC waves. *Frontiers in Astronomy and Space Sciences*, 8, 719715. <https://doi.org/10.3389/fspas.2021.719715>
- Lessard, M. R., Paulson, K., Spence, H. E., Weaver, C., Engebretson, M. J., Millan, R., et al. (2019). Generation of EMIC waves and effects on particle precipitation during a solar wind pressure intensification with $B_z > 0$. *Journal of Geophysical Research: Space Physics*, 124(6), 4492–4508. <https://doi.org/10.1029/2019JA026477>
- Li, Z., Millan, R. M., Hudson, M. K., Woodger, L. A., Smith, D. M., Chen, Y., et al. (2014). Investigation of EMIC wave scattering as the cause for the BARREL 17 January 2013 relativistic electron precipitation event: A quantitative comparison of simulation with observations. *Geophysical Research Letters*, 41(24), 8722–8729. <https://doi.org/10.1002/2014GL062273>
- Loto'aniu, T. M., Fraser, B. J., & Waters, C. L. (2009). The modulation of electromagnetic ion cyclotron waves by Pc 5 ULF waves. *Annales Geophysicae*, 27(1), 121–130. <https://doi.org/10.5194/angeo-27-121-2009>
- Mace, R. L., Sydora, R. D., & Silin, I. (2011). Effects of superthermal ring current ion tails on the electromagnetic ion cyclotron instability in multi-ion magnetospheric plasmas. *Journal of Geophysical Research*, 116(A5), A05206. <https://doi.org/10.1029/2010JA016393>
- McCollough, J. P., Elkington, S. R., & Baker, D. N. (2012). The role of Shabansky orbits in compression-related electromagnetic ion cyclotron wave growth. *Journal of Geophysical Research*, 117(A1), A01208. <https://doi.org/10.1029/2011JA016948>
- McCollough, J. P., Elkington, S. R., Usanova, M. E., Mann, I. R., Baker, D. N., & Kale, Z. C. (2010). Physical mechanisms of compressional EMIC wave growth. *Journal of Geophysical Research*, 115(A10), A10214. <https://doi.org/10.1029/2010JA015393>
- Meredith, N. P., Horne, R. B., Kersten, T., Fraser, B. J., & Grew, R. S. (2014). Global morphology and spectral properties of EMIC waves derived from CRRES observations. *Journal of Geophysical Research*, 119(7), 5328–5342. <https://doi.org/10.1002/2014JA020064>
- Meredith, N. P., Thorne, R. M., Horne, R. B., Summers, D., Fraser, B. J., & Anderson, R. R. (2003). Statistical analysis of relativistic electron energies for cyclotron resonance with EMIC waves observed on CRRES. *Journal of Geophysical Research*, 108(A6), 1250. <https://doi.org/10.1029/2002JA009700>
- Millan, R. M., & Thorne, R. M. (2007). Review of radiation belt relativistic electron losses. *Journal of Atmospheric and Solar-Terrestrial Physics*, 69(3), 362–377. <https://doi.org/10.1016/j.jastp.2006.06.019>
- Min, K., Lee, J., Keika, K., & Li, W. (2012). Global distribution of EMIC waves derived from THEMIS observations. *Journal of Geophysical Research*, 117(A5), A05219. <https://doi.org/10.1029/2012JA017515>
- Min, K., Liu, K., Bonnell, J. W., Breneman, A. W., Denton, R. E., Funsten, H. O., et al. (2015). Study of EMIC wave excitation using direct ion measurements. *Journal of Geophysical Research: Space Physics*, 120(4), 2702–2719. <https://doi.org/10.1002/2014JA020717>
- Mithaiwala, M., Crabtree, C., Ganguli, G., Rudakov, L., & Keika, K. (2013). Convective amplification of electromagnetic ion cyclotron waves from ring-distribution protons in the inner magnetosphere. *Journal of Geophysical Research: Space Physics*, 118(12), 7538–7544. <https://doi.org/10.1002/2013JA019134>
- Morley, S. K., Ables, S. T., Sciffer, M. D., & Fraser, B. J. (2009). Multipoint observations of Pc1-2 waves in the afternoon sector. *Journal of Geophysical Research*, 114(A9), A09205. <https://doi.org/10.1029/2009JA014162>
- Mursula, K. (2007). Satellite observations of Pc1 pearl waves: The changing paradigm. *Journal of Atmospheric and Solar-Terrestrial Physics*, 69(14), 1623–1634. <https://doi.org/10.1016/j.jastp.2007.02.013>
- Mursula, K., Blomberg, L. G., Lindqvist, P.-A., Marklund, G. T., Bräysy, T., Rasinkangas, R., & Tanskanen, P. (1994). Dispersive Pc1 bursts observed by Freja. *Geophysical Research Letters*, 21(17), 1851–1854. <https://doi.org/10.1029/94GL01584>
- Nakamura, S., Omura, Y., & Angelopoulos, V. (2016). A statistical study of EMIC rising and falling tone emissions observed by THEMIS. *Journal of Geophysical Research: Space Physics*, 121(9), 8374–8391. <https://doi.org/10.1002/2016JA022353>
- Nakamura, S., Omura, Y., Kletzing, C., & Baker, D. N. (2019). Rapid precipitation of relativistic electron by EMIC rising-tone emissions observed by the Van Allen Probes. *Journal of Geophysical Research: Space Physics*, 124(8), 6701–6714. <https://doi.org/10.1029/2019JA026772>
- Nakamura, S., Omura, Y., Machida, S., Shoji, M., Nosé, M., & Angelopoulos, V. (2014). Electromagnetic ion cyclotron rising tone emissions observed by THEMIS probes outside the plasmopause. *Journal of Geophysical Research: Space Physics*, 119(3), 1874–1886. <https://doi.org/10.1002/2013JA019146>
- Nakamura, S., Omura, Y., Shoji, M., Nosé, M., Summers, D., & Angelopoulos, V. (2015). Subpacket structures in EMIC rising tone emissions observed by the THEMIS probes. *Journal of Geophysical Research: Space Physics*, 120(9), 7318–7330. <https://doi.org/10.1002/2014JA020764>

- Ni, B., Bortnik, J., Thorne, R. M., Ma, Q., & Chen, L. (2013). Resonant scattering and resultant pitch angle evolution of relativistic electrons by plasmaspheric hiss. *Journal of Geophysical Research: Space Physics*, *118*(12), 7740–7751. <https://doi.org/10.1002/2013JA019260>
- Nomura, R., Shiokawa, K., Omura, Y., Ebihara, Y., Miyoshi, Y., Sakaguchi, K., et al. (2016). Pulsating proton aurora caused by rising tone Pc1 waves. *Journal of Geophysical Research: Space Physics*, *121*(2), 1608–1618. <https://doi.org/10.1002/2015JA021681>
- Nosé, M., Oimatsu, S., Keika, K., Kletzing, C. A., Kurth, W. S., De Pascuale, S., et al. (2015). Formation of the oxygen torus in the inner magnetosphere: Van Allen Probes observations. *Journal of Geophysical Research: Space Physics*, *120*(2), 1182–1196. <https://doi.org/10.1002/2014JA020593>
- Omura, Y., Pickett, J., Grison, B., Santolik, O., Dandouras, I., Engebretson, M., et al. (2010). Theory and observation of electromagnetic ion cyclotron triggered emissions in the magnetosphere. *Journal of Geophysical Research*, *115*(A7), A07234. <https://doi.org/10.1029/2010JA015300>
- Omura, Y., & Summers, D. (2006). Dynamics of high-energy electrons interacting with whistler mode chorus emissions in the magnetosphere. *Journal of Geophysical Research*, *111*(A9), A09222. <https://doi.org/10.1029/2006JA011600>
- Paulson, K. W., Smith, C. W., Lessard, M. R., Engebretson, M. J., Torbert, R. B., & Kletzing, C. A. (2014). In situ observations of Pc1 pearl pulsations by the Van Allen Probes. *Geophysical Research Letters*, *41*(6), 1823–1829. <https://doi.org/10.1002/2013GL059187>
- Paulson, K. W., Smith, C. W., Lessard, M. R., Torbert, R. B., Kletzing, C. A., & Wygant, J. R. (2017). In situ statistical observations of Pc1 pearl pulsations and unstructured EMIC waves by the Van Allen Probes. *Journal of Geophysical Research: Space Physics*, *122*(1), 105–119. <https://doi.org/10.1002/2016JA023160>
- Pickett, J. S., Grison, B., Omura, Y., Engebretson, M. J., Dandouras, I., Masson, A., et al. (2010). Cluster observations of EMIC triggered emissions in association with Pc1 waves near Earth's plasmapause. *Geophysical Research Letters*, *37*(9), L09104. <https://doi.org/10.1029/2010GL042648>
- Qin, M., Hudson, M. K., Li, Z., Millan, R. M., Shen, X.-C., Shprits, Y. Y., et al. (2019). Investigating loss of relativistic electrons associated with EMIC waves at low L values on 22 June 2015. *Journal of Geophysical Research: Space Physics*, *124*(6), 4022–4036. <https://doi.org/10.1029/2018JA025726>
- Remya, B., Sibeck, D. G., Halford, A. J., Murphy, K. R., Reeves, G. D., Singer, H. J., et al. (2018). Ion injection triggered EMIC waves in the Earth's magnetosphere. *Journal of Geophysical Research: Space Physics*, *123*(6), 4921–4938. <https://doi.org/10.1029/2018JA025354>
- Saikin, A. A., Zhang, J.-C., Allen, R. C., Smith, C. W., Kistler, L. M., Spence, H. E., et al. (2015). The occurrence and wave properties of H⁺-He⁺- and O⁺-band EMIC waves observed by the Van Allen Probes. *Journal of Geophysical Research: Space Physics*, *120*(9), 7477–7492. <https://doi.org/10.1002/2015JA021358>
- Saikin, A. A., Zhang, J.-C., Smith, C. W., Spence, H. E., Torbert, R. B., & Kletzing, C. A. (2016). The dependence on geomagnetic conditions and solar wind dynamic pressure of the spatial distributions of EMIC waves observed by the Van Allen Probes. *Journal of Geophysical Research: Space Physics*, *121*(5), 4362–4377. <https://doi.org/10.1002/2016JA022523>
- Sakaguchi, K., Kasahara, Y., Shoji, M., Omura, Y., Miyoshi, Y., Nagatsuma, T., et al. (2013). Akebono observations of EMIC waves in the slot region of the radiation belts. *Geophysical Research Letters*, *40*(21), 5587–5591. <https://doi.org/10.1002/2013GL058258>
- Santolik, O., Parrot, M., & Lefeuvre, F. (2003). Singular value decomposition methods for wave propagation analysis. *Radio Science*, *38*(1), 1010. <https://doi.org/10.1029/2000rs002523>
- Shoji, M., Miyoshi, Y., Katoh, Y., Keika, K., Angelopoulos, V., Kasahara, S., et al. (2017). Ion hole formation and nonlinear generation of electromagnetic ion cyclotron waves: THEMIS observations. *Geophysical Research Letters*, *44*(17), 8730–8738. <https://doi.org/10.1002/2017GL074254>
- Shoji, M., & Omura, Y. (2011). Simulation of electromagnetic ion cyclotron triggered emissions in the Earth's inner magnetosphere. *Journal of Geophysical Research*, *116*(A5), A05212. <https://doi.org/10.1029/2010JA016351>
- Shoji, M., & Omura, Y. (2012). Precipitation of highly energetic protons by helium branch electromagnetic ion cyclotron triggered emissions. *Journal of Geophysical Research*, *117*(A12), A12210. <https://doi.org/10.1029/2012JA017933>
- Shoji, M., & Omura, Y. (2013). Triggering process of electromagnetic ion cyclotron rising tone emissions in the inner magnetosphere. *Journal of Geophysical Research: Space Physics*, *118*(9), 5553–5561. <https://doi.org/10.1002/jgra.50523>
- Shoji, M., & Omura, Y. (2017). Nonlinear generation mechanism of EMIC falling tone emissions. *Journal of Geophysical Research: Space Physics*, *122*(10), 9924–9933. <https://doi.org/10.1002/2017JA023883>
- Shoji, M., Omura, Y., Grison, B., Pickett, J., Dandouras, I., & Engebretson, M. (2011). Electromagnetic ion cyclotron waves in the helium branch induced by multiple electromagnetic ion cyclotron triggered emissions. *Geophysical Research Letters*, *38*(17), L17102. <https://doi.org/10.1029/2011GL048427>
- Sigsbee, K., Kletzing, C. A., Faden, J. B., Jaynes, A. N., Reeves, G. D., & Jahn, J.-M. (2020). Simultaneous observations of electromagnetic ion cyclotron (EMIC) waves and pitch angle scattering during a Van Allen Probes conjunction. *Journal of Geophysical Research: Space Physics*, *125*(4), e2019JA027424. <https://doi.org/10.1029/2019JA027424>
- Sigsbee, K., Kletzing, C. A., Smith, C. W., MacDowall, R., Spence, H., Reeves, G., et al. (2016). Van Allen Probes, THEMIS, GOES, and Cluster observations of EMIC waves, ULF pulsations, and an electron flux dropout. *Journal of Geophysical Research: Space Physics*, *121*(3), 1990–2008. <https://doi.org/10.1002/2014JA020877>
- Storey, L. R. O. (1953). An investigation of whistling atmospherics. *Philosophical Transactions of the Royal Society of London*, *246*, 113–141.
- Teng, S., Li, W., Tao, X., Ma, Q., & Shen, X. (2019). Characteristics and generation of low-frequency magnetosonic waves below the proton gyrofrequency. *Geophysical Research Letters*, *46*(21), 11652–11660. <https://doi.org/10.1029/2019GL085372>
- Tetrick, S. S., Engebretson, M. J., Posch, J. L., Olson, C. N., Smith, C. W., Denton, R. E., et al. (2017). Location of intense electromagnetic ion cyclotron (EMIC) wave events relative to the plasmapause: Van Allen Probes observations. *Journal of Geophysical Research: Space Physics*, *122*(4), 4064–4088. <https://doi.org/10.1002/2016JA023392>
- Thorne, R. (2010). Radiation belt dynamics: The importance of wave-particle interactions. *Geophysical Research Letters*, *37*(22), L22107. <https://doi.org/10.1029/2010GL044990>
- Thorne, R., & Horne, R. (1994). Energy transfer between energetic ring current H⁺ and O⁺ by electromagnetic ion cyclotron waves. *Journal of Geophysical Research*, *99*(A9), 17275–17282. <https://doi.org/10.1029/94ja01007>
- Thorne, R., & Kennel, C. (1971). Relativistic electron precipitation during magnetic storm main phase. *Journal of Geophysical Research*, *76*(19), 4446–4453. <https://doi.org/10.1029/ja076i019p04446>
- Ukhorskiy, A. Y., Shprits, Y. Y., Anderson, B. J., Takahashi, K., & Thorne, R. M. (2010). Rapid scattering of radiation belt electrons by storm-time EMIC waves. *Geophysical Research Letters*, *37*(9), L09101. <https://doi.org/10.1029/2010GL042906>
- Usanova, M. E. (2021). Energy exchange between electromagnetic ion cyclotron (EMIC) waves and thermal plasma: From theory to observations. *Frontiers in Astronomy and Space Sciences*, *8*, 744344. <https://doi.org/10.3389/fspas.2021.744344>
- Usanova, M. E., Drozdov, A., Orlova, K., Mann, I. R., Shprits, Y., Robertson, M. T., et al. (2014). Effect of EMIC waves on relativistic and ultrarelativistic electron populations: Ground based and Van Allen Probes observations. *Geophysical Research Letters*, *41*(5), 1375–1381. <https://doi.org/10.1002/2013GL059024>

- Usanova, M. E., Malaspina, D. M., Jaynes, A. N., Bruder, R. J., Mann, I. R., Wygant, J. R., & Ergun, R. E. (2016). Van Allen Probes observations of oxygen cyclotron harmonic waves in the inner magnetosphere. *Geophysical Research Letters*, *43*(17), 8827–8834. <https://doi.org/10.1002/2016GL070233>
- Usanova, M. E., Mann, I. R., Bortnik, J., Shao, L., & Angelopoulos, V. (2012). THEMIS observations of electromagnetic ion cyclotron wave occurrence: Dependence on AE, SYMH, and solar wind dynamic pressure. *Journal of Geophysical Research*, *117*(A10), A10218. <https://doi.org/10.1029/2012JA018049>
- Usanova, M. E., Mann, I. R., Kale, Z. C., Rae, I. J., Sydora, R. D., Sandanger, M., et al. (2010). Conjugate ground and multisatellite observations of compression-related EMIC Pc1 waves and associated proton precipitation. *Journal of Geophysical Research*, *115*(A7), A07208. <https://doi.org/10.1029/2009JA014935>
- Usanova, M. E., Mann, I. R., Rae, I. J., Kale, Z. C., Angelopoulos, V., Bonnell, J. W., et al. (2008). Multipoint observations of magnetospheric compression-related EMIC Pc1 waves by THEMIS and CARISMA. *Geophysical Research Letters*, *35*(17), L17S25. <https://doi.org/10.1029/2008GL034458>
- Wang, X. Y., Huang, S. Y., Allen, R. C., Fu, H. S., Deng, X. H., Zhou, M., et al. (2017). The occurrence and wave properties of EMIC waves observed by the Magnetospheric Multiscale (MMS) mission. *Journal of Geophysical Research: Space Physics*, *122*(8), 8228–8240. <https://doi.org/10.1002/2017JA024237>
- Yu, X., Yuan, Z., Wang, D., Li, H., Huang, S., Wang, Z., et al. (2015). In situ observations of EMIC waves in O⁺ band by the Van Allen Probe A. *Geophysical Research Letters*, *42*(5), 1312–1317. <https://doi.org/10.1002/2015GL063250>
- Yuan, Z., Deng, X., Lin, X., Peng, Y., Zhou, M., Décréau, P. M. E., et al. (2012). Link between EMIC waves in plasmaspheric plume and a detached sub-auroral proton arc with observations of Cluster and IMAGE satellites. *Geophysical Research Letters*, *37*(7), L07108. <https://doi.org/10.1029/2010GL042711>
- Yuan, Z., Li, M., Xiong, Y., Li, H., Zhou, M., Wang, D., et al. (2013). Simultaneous observations of precipitating radiation belt electrons and ring current ions associated with the plasmaspheric plume. *Journal of Geophysical Research*, *118*(7), 4391–4399. <https://doi.org/10.1002/jgra.50432>

Erratum

In the originally published version of this article, the color and line weights in Figures 8 and 13 were not correct. These errors have been corrected, and this may be considered the authoritative version of record.